Fuel 241 (2019) 372–381

Contents lists available at ScienceDirect

Fuel

journal homepage: www.elsevier.com/locate/fuel

Full Length Article

Gasification performance of *Spirulina* microalgae – A thermodynamic study with tar formation

Muflih A. Adnan[a,c,1], Qingang Xiong[b,1], Arif Hidayat[a], Mohammad M. Hossain[c,d,*]

[a] Department of Chemical Engineering, Islamic University of Indonesia, Sleman, Daerah Istimewa Yogyakarta 55584, Indonesia
[b] IT Innovation Center, General Motors, Warren, MI 48092, USA
[c] Department of Chemical Engineering, King Fahd University of Petroleum & Minerals, Dhahran 31261, Saudi Arabia
[d] Center of Research Excellence in Nanotechnology, King Fahd University of Petroleum & Minerals, Dhahran 31261, Saudi Arabia

ARTICLE INFO

Keywords:
Biomass gasification
Spirulina microalgae
Tar formation
Thermodynamic analysis
Optimization

ABSTRACT

In this work, the performance of a novel configuration for *Spirulina* microalgae gasification was investigated through an improved thermodynamic model using Aspen Plus. Compared with existing thermodynamic models, tar formation is included in the improved counterpart. The proposed novel gasification process consists of four primary zones: (i) pyrolysis, (ii) combustion, (iii) gasification, and (iv) optimization. First, the modeling results were compared against experimental values, where a good agreement (relative error < 10%) was obtained under identical operating conditions. Then, performance of the novel gasification configuration was studied using the developed improved thermodynamic model at various operating conditions. Metrics such as gasification system efficiency, syngas composition and cold gas efficiency were used to measure the performance. It was found that incorporation of the optimization zone improves the concentration of CO and H_2 at the controlled use of gasifying agents. Moreover, injection of suitable amount of gasifying agents enhances the gasification performance. Finally, the effects of O_2 equivalence ratio and steam injection on the system performance were investigated.

1. Introduction

In recent years, besides traditional agricultural biomass, a special type of biomass, microalgae, has received considerable attention as a clean energy source to substitute fossil fuels due to the increased concern on energy security as well as environmental sustainability [1]. Biomass from different sources including terrestrial biomass and marine biomass is considered as a potential candidate to substitute the fossil fuels given its advantages over fossil fuels in term of environment issue (e.g., carbon neutral cycle). Recently, on purpose marine biomass such as microalgae has received a growing attention as a clean energy source attributable to its advantages over terrestrial biomass including its ability to recover CO_2 through photosynthesis way during their growing period, tolerance with nutrients in the water, higher photosynthesis efficiency and shorter growth cycle [2]. The use of microalgae emits notably low SO_x emission due to its minimum concentration of sulfur. In addition, even microalgae consists of high-protein, indicating considerable amount of nitrogen element, the NO_x formation during gasification process could be minimized by selecting proper gasifying agent (i.e., O_2, CO_2) [3,4]. Indeed, production cost of microalgae is a major consideration for commercialization of microalgae for biofuels. The selection of proper nutrients, water and CO_2 could potentially cut the production cost by > 50% [5]. Furthermore, the production cost can be reduced by taking suitable land for cultivation of microalgae [6] and the harvesting method [7]. Among various approaches to convert microalgae into biofuels, gasification through which a mixture of incondensable gas such as H_2, CO, CH_4 and CO_2 is produced, has been widely viewed as a promising way due to its relatively high energy conversion efficiency [2].

However, at industrial scale, effective gasification of microalgae is still limited largely due to the existence of tar, a complex mixture of aromatic hydrocarbons [8]. Because of the existence of tar which comes out along with the produced incondensable gas, gasification efficiency can be significantly diminished [9]. Therefore, tar concentration during the gasification of microalgae should be kept as minimum as possible. In most instances, tar concentration can be reduced using separation either by dry treatment (i.e., cyclone, filters, etc.) or wet treatment (i.e., spray towers, wet cyclones, etc.). Although separation has been

* Corresponding author at: Department of Chemical Engineering, King Fahd University of Petroleum & Minerals, Dhahran 31261, Saudi Arabia.
E-mail address: mhossain@kfupm.edu.sa (M.M. Hossain).
[1] These authors contributed equally to this work.

https://doi.org/10.1016/j.fuel.2018.12.061
Received 1 September 2018; Received in revised form 10 December 2018; Accepted 11 December 2018
Available online 18 December 2018
0016-2361/

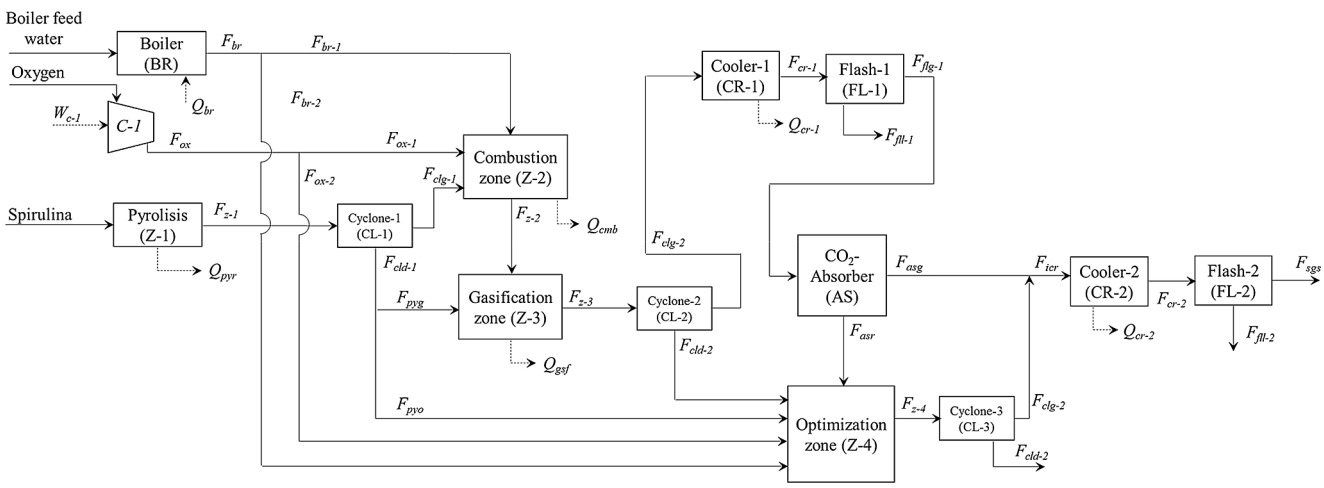

Fig. 1. Schematic diagram of the proposed gasification process for *Spirulina*.

demonstrated as an effective way to remove tar from the produced incondensable gas, it is not able to fully preserve the high gasification efficiency given tar is wasted instead of being converted to incondensable gas [10]. Moreover, post-processing the separated tar requires additional energy, which will further decrease the overall gasification efficiency [1,11]. Thus, it is more feasible to directly convert tar into incondensable combustible gas.

During microalgae gasification, tar is primarily formed in the pyrolysis step which occurs at relatively low temperature. In principle, direct conversion of tar into incondensable combustible gas can be achieved through three approaches, i.e., (i) increasing the gasification temperature, (ii) employment of tar cracking catalysts, and (iii) novel gasifier design. However, thermal cracking of tar at high temperature is costly as this is an energy intensive process [1,12]. In general, using catalysts should be a proper way to increase tar conversion at relatively low temperature [1,13]. However, it is highly possible for catalysts to suffer from the problems of deactivation due to pore blockage by coke and degradation of mechanical strengths [14–16]. For design of novel gasifiers, in recent years many investigations have shown that it is an efficient way to increase tar conversion and gasification efficiency. For example, Susanto and Beenackers [17] proposed a new design on a continuous downdraft gasifier for woody biomass, in which an internal cycle is introduced. With such novel design, tar produced from the pyrolysis zone is cracked in the combustion zone, through which the final collected tar concentration decreases by 97% (from 1410 mg·Nm^{-3} to 48 mg·Nm^{-3}). Similarly, Brandt et al. [18] successfully reduced tar content below 15 mg·Nm^{-3} using the design of two-stage gasifier with a dry wood as the feedstock. Therefore, it could be anticipated that novel design of gasifier could significantly increase the efficiency of microalgae gasification.

In our previous work [19], a gasification system including a CO_2-absorber to upgrade the syngas quality by removing CO_2 from the syngas stream was proposed and assessed. It was proved to be very efficient for microalgae gasification. In this study, such novel gasification design is further enhanced by realizing the in-situ utilization of pure CO_2 as the side product through facilitating the Bouduard reaction to enhance the char and CO_2 conversion into CO, which is usually used in a direct carbon solid oxide fuel cell (SOFC) [20]. The improved configuration consists of pyrolysis, combustion, gasification, and optimization stages, respectively, with a number of advantages such as production of clean syngas due to an effective tar conversion and in-situ utilization of CO_2.

Assessing the performance of a novel design for microalgae gasification is critical to its subsequent optimization and scale-up processes. However, it is rather difficult, even if possible, to use the traditional experimental approach to conduct such laborious, high-cost and time-consuming work, especially for a large-scale microalgae gasification [21]. Thermodynamic modeling, where steady-state equilibrium physicochemical principles are applied to predict the overall reactor outcome, has been widely viewed as a promising way to quickly estimate the overall performance of biomass gasification with reasonable accuracy [22–25]. For this reason, thermodynamic modeling has also been largely employed to simulate biomass gasification and evaluate the performance of novel gasifier designs [26,27]. This is also the case to microalgae gasification [22,23]. However, most thermodynamic modeling of microalgae gasification uses relatively simplified reactions to model the tar formation and conversion. This will definitely lower the overall prediction accuracy for thermodynamic modeling of microalgae gasification. Due to the high nitrogenated content in microalgae, many studies have revealed that it is reasonable to approximate tar as nitrogenated aromatic hydrocarbon to preserve engineering accuracy [28,29]. Therefore, such tar approximation is adopted in our current thermodynamic modeling of microalgae gasification [30].

In this work, a comprehensive thermodynamic modeling of the foregoing mentioned new configuration for microalgae gasification was conducted using Aspen Plus. The single-species microalgae, *Spirulina*, was selected as the feedstock and tar was modeled as a mixture of nitrogenated aromatic hydrocarbons. *Spirulina* contains high concentration of protein, which is favorable for production of oil during pyrolysis stage [31]. Furthermore, the vaporized oil is converted into syngas as the major gasification product. First, the thermodynamic modeling was validated against experimental results to prove its accuracy. Then, performance of the new *Spirulina* gasification system was analyzed with respect to gasification system efficiency, syngas composition and cold gas efficiency. Finally, the flow rates of oxygen and steam were varied to investigate their effects on gasification performance for optimal operation of the new design.

2. Description of the novel design

The proposed novel design of microalgae gasification process is shown in Fig. 1, where four major zones are involved, i.e., pyrolysis zone, combustion zone, gasification zone, and optimization zone. The gasifying agents are steam and high-purity oxygen. The ultimate and proximate analysis of the feedstock *Spirulina* including its heating value are summarized in Table 1. The *Spirulina* feedstock including its properties (i.e., ultimate, proximate and high heating value) for simulation is adapted from the one used by Hong et al. [31]. The actual operation of *Spirulina* gasification in this novel configuration can be majorly described as follows. At the inlet, *Spirulina* is continuously fed at constant flow rate of 100 kg/h. The feedstock first enters the pyrolysis zone (Z-1). In Z-1, moisture content in *Spirulina* evaporates first due to high

Table 1
Properties of *Spirulina* [31].

Proximate, % mass	
Moisture	6.7
Volatile matters	73.5
Fixed carbon	13.2
Ash	6.6
Ultimate, % mass	
C	49.8
H	6.6
O	31.9
N	11.0
S	0.7
HHV, MJ/kg	15.1

temperature. Then, *Spirulina* is decomposed into solid (i.e., char) and gaseous products including water vapor, permanent gases (CO, H_2, CH_4 and CO_2) and tars. These pyrolysis products are sent to the cyclone 1 (CL-1) to separate the solid products from the gaseous products. The solid products are further split into two streams: one to the gasification zone (Z-3) and the other to the optimization zone (Z-4). At the same time, the gaseous products are directed to the combustion zone (Z-2). In Z-2, the gaseous products contact with the gasifying agents and the tar concentration decays due to its conversion to permanent gases. After that, the products from Z-2 are sent to Z-3, where they interact with a portion of char obtained from CL-1. The gasification products are then directed to cyclone-2 (CL-2) to remove the unconverted char. Later, the solid products are directed to Z-4 while the gaseous products are cooled in the cooler-1 (CR-1). The condensed water from CR-1 is separated in the flash-1 (FL-1) before it is fed to the CO_2-absorber (AS) unit, where the CO_2 is removed from the cooled dry gaseous gasification products. The high-purity CO_2 is directed to Z-4 while other gaseous gasification products are sent to the cooler-2 (CR-2), along with the gas from the cyclone-3 (CL-3). In Z-4, the high-purity CO_2 reacts with a portion of char received from CL-1 and part of gasifying agents (i.e., O_2 and steam). The condensed water from CR-2 is removed in the flash-2 (FL-2) before distributing the syngas to the users. The overall gasification process as described above except the pyrolysis phase majorly contains the following reactions [30]:

Partial oxidation $$C + \frac{1}{2}O_2 \leftrightarrow CO \quad (1)$$

Boudouard reaction $$C + CO_2 \leftrightarrow 2CO \quad (2)$$

Steam reforming $$C + H_2O \leftrightarrow CO + H_2 \quad (3)$$

Water-gas shift reaction $$CO + H_2O \leftrightarrow CO_2 + H_2 \quad (4)$$

Methane reforming $$CH_4 + H_2O \leftrightarrow CO + 3H_2 \quad (5)$$

CO_2 reforming $$CH_4 + CO_2 \leftrightarrow 2CO + 2H_2 \quad (6)$$

Steam reforming of aromatic $$C_xH_yN_z + xH_2O \leftrightarrow xCO + \frac{1}{2}(y + 2x)H_2 + \frac{1}{2}zN_2 \quad (7)$$

p-Cresol steam reforming $$C_7H_8O + 6H_2O \leftrightarrow 7CO + 10H_2 \quad (8)$$

Phenol steam reforming $$C_6H_5OH + 5H_2O \leftrightarrow 6CO + 8H_2 \quad (9)$$

Naphthalene steam reforming $$C_{10}H_8 + 10H_2O \leftrightarrow 10CO + 14H_2 \quad (10)$$

Alkane combustion $$C_nH_{2n+2} + \frac{1}{2}(3n + 1)O_2 \leftrightarrow nCO_2 + (n + 1)H_2O \quad (11)$$

CO combustion $$CO + \frac{1}{2}O_2 \leftrightarrow CO_2 \quad (12)$$

Methane formation $$C + 2H_2 \leftrightarrow CH_4 \quad (13)$$

3. Model development

Performance of the proposed novel gasification process for *Spirulina* is modeled using AspenPlus®, primarily based on the minimization of Gibbs free energy [23,32]. In the simulation, the feedstock *Spirulina* is classified as a nonconventional element while the gasifying agents are categorized as conventional elements. Regarding the solid products, carbon and ash are modeled as cisolid and nonconventional elements, respectively. The gaseous products including H_2, H_2O, CO, CO_2, CH_4, C_2H_6 and tar are considered as conventional elements. It is worth noting that the tar in this simulation is represented by a mixture of indole, benzyl nitrile, benzonitrile, quinolone, p-cresol, phenol and naphthalene. The Peng-Robinson equation of state is chosen as the thermodynamic model due to its good accuracy for simulation of gasification process [23,30,33]. The following assumptions are made: (i) ash is inert; (ii) mass transfer limitation is minimum; and (iii) pressure drop along the equipment is trivial. Operating parameters of the proposed novel gasification process for *Spirulina* are listed in Table 2. The efficiency of the rotating equipment is adapted from the previous literature [19]. In the following, detailed information on the thermodynamic modeling of zones from pyrolysis to optimization is described.

3.1. Pyrolysis zone (Z-1)

Spirulina enters Z-1 with constant mass flow rate of 100 kg/h. In Z-1, the feedstock is thermally decomposed into (a) gaseous products (conventional elements) including H_2, H_2O, CO, CO_2, CH_4, C_2H_6 and tar, (b) carbon (ci-solid element), and (c) ash (nonconventional element). For the thermodynamic modeling of Z-1, the following assumptions are made:

(i) The char only consists of carbon and ash. This has been confirmed through experiment by Fagbemi et al. [34], reporting that a large content of carbon (> 88 wt%) is observed on the char from pyrolysis at 773 K.
(ii) The amount of char is calculated based on the experimental value suggested by Hong et al. [31], showing the char yield from pyrolysis at 973 K.
(iii) The tar is limited to indole, benzyl nitrile, benzonitrile, quinolone, p-cresol, phenol and naphthalene. This is based on the experimental results from Hong et al. [31], where tar was found to be almost composed of nitrogenated compounds, phenols, and polycyclic aromatic hydrocarbons during pyrolysis at 973 K.
(iv) Due to the extreme complexity of the nitrogenated compounds, their thermochemical properties are obtained using the empirical relationship proposed by Benson et al. [35].

The quantity of products as well as heat needed are predicted by

Table 2
Operating conditions of the proposed novel gasification process for *Spirulina* in the simulation.

Inlet temperature of *Spirulina*, boiler feed water and O_2	298 K
Temperature of steam entering gasification zone	623 K
Temperature of pyrolysis zone (Z-1)	973 K
Temperature of combustion zone (Z-2)	1523 K
Temperature of gasification zone (Z-3)	1423 K
Temperature of optimization zone (Z-4)	873 K
Efficiency of BFW pump	0.80
O_2 compressor	
Isentropic efficiency	0.85
Mechanical efficiency	0.96

solving the elemental and heat balances simultaneously in the RYield.

3.2. Combustion zone (Z-2)

The gaseous products obtained from Z-1 then pass CL-1 and contact with the gasifying agents in Z-2, undergoing exothermic reactions which implies to high operating temperature (1523 K). Due to the high temperature in Z-2, reactions in this zone are assumed to reach equilibrium very fast. Therefore, the RGibss block is taken to represent Z-2 in the simulation. RGibss is the only Aspen Plus block which operates according to the minimization of Gibbs free energy method. The products obtained from Z-2 are sent to Z-3 for further processing.

3.3. Gasification zone (Z-3)

In Z-3, the hot gases received from Z-2 react with the solid pyrolysis products from CL-1, resulting in a set of endothermic reactions. Consequently, the temperature of Z-3 is slightly lower than its counterpart in Z-2, as shown in Table 2. However, the temperature in Z-3 is still considered to be adequate to achieve equilibrium. Therefore, the RGibbs block can still be properly used to model Z-3. The products from Z-3 are sent to the gas separation process to remove CO_2 from the syngas stream.

3.4. Optimization zone (Z-4)

The CO_2 from the CO_2-absorber (AS) unit reacts with the unconverted char received from CL-2. In addition, part of char obtained from CL-1 and part of gasifying agents is directed to Z-4. The endothermic reactions in Z-4 lead to the decrease of the operating temperature. Again, an equilibrium condition is assumed to occur at this temperature, where the RGibbs block is employed to model Z-4.

4. Performance evaluation

Performance of a gasification process is usually assessed based on the following aspects: (i) concentration of the targeted syngas products (i.e., primarily H_2 and CO), (ii) cold gas efficiency (CGE), and (iii) gasification system efficiency (GSE). Composition of the syngas is expressed in terms of dry gas basis. The CGE designates the ratio of serviceable energy in the syngas to the reserved energy in the feedstock and steam, which can be expressed as

$$CGE(-) = \frac{m_{sgs} \cdot LHV_{sgs}}{m_{ms} \cdot LHV_{ms} + H_{sm} \cdot m_{sm}}, \tag{14}$$

where m H, and LHV are the mass flow rate, enthalpy and the lower heating value, respectively. The subscript *sgs, ms* and *sm* represent the syngas, *Spirulina* and steam, respectively.

GSE accounts for the efficiency of the whole gasification system, which is expressed as

$$GSE = \frac{m_{sgs} \times LHV_{sgs} + Q_{cr-1} + Q_{cr-2}}{m_{ms} \times LHV_{ms} + Q_{z-1} + Q_{z-2} + Q_{z-3} + Q_{z-4} + Q_{br} + E_{c-1} + E_{ox} + E_{as}}, \tag{15}$$

where Q and E are the heat rate and energy rate, respectively. The use of relatively purified O_2 (95% O_2) for gasification is favorable due to its ability to provide a higher gasification temperature which leads to a higher conversion of tar reforming, compared with air [17,30]. Consequently, additional energy of 305 kWh per ton of O_2 is required for the gasification process [36]. An extra energy consumption of 3 MJ/kg of CO_2 absorbed is also involved to run the amine-based CO_2 absorber with the CO_2 removal efficiency of 90% [37].

5. Model validation

The proposed thermodynamic model was first validated by comparing the predicted solid and gaseous pyrolysis products with those of the experimental data reported by Hong et al. [31]. Simulation conditions were set the same as those in the corresponding experiment [31]. The product yields after the pyrolysis stage are summarized Table 3. It can be clearly seen that the proposed thermodynamic model satisfactorily predicts the yield of each product. It is worth noting that the formation of tar is also predicted in this model. As mentioned earlier, tar consists of complex compounds when compared with other specific gaseous products. In addition, the concentration of tar in the syngas is considerably smaller than other species. Therefore, the difference of tar concentration between experiment and this model is reasonable if the above two factors are taken into account.

Table 3
Gas composition of the experimental work [38] and the model.

Compound	Hong et al. [31]	This work	Error (%)
Gaseous product, mol%			
H_2	32.6%	33.4%	2.4%
CO	40.5%	37.8%	6.6%
CH_4	13.8%	15.1%	9.0%
CO_2	7.9%	6.7%	15.4%
C_2H_6	3.0%	3.7%	24.2%
Tar	1.2%	1.5%	24.2%
Solid product, wt%			
Char	10.0%	10.9%	9.4%

6. Results and discussion

The proposed novel gasification configuration is first evaluated by the foregoing developed thermodynamic model, at a constant feedstock feed rate of 100 kg/h. The temperatures of the pyrolysis zone (Z-1), combustion zone (Z-2), gasification zone (Z-3), and optimization zone (Z-4) are maintained constant at 973 K, 1523 K, 1423 K and 873 K, respectively. Then, the effects of O_2 equivalence ratio and steam injection on process performance are investigated.

6.1. Process description

As mentioned above, the overall gasification process consists of four primary steps, in which the pyrolysis step converts the *Spirulina* feedstock into char and pyrolysis gas products, the combustion step reforms tar into the desired permanent gases, the gasification step converts char into syngas and the optimization step transforms unconverted char into valuable gases with the help of the recycled CO_2. Pure oxygen and steam are fed into the system with an oxygen equivalence ratio (O_2 ER ratio) of 0.3 and steam to carbon (S/C) ratio of 1.0. The O_2 ER ratio defined as the ratio of actual oxygen to biomass ratio to the stoichiometric oxygen to biomass ratio. The S/C ratio is the molar ratio of steam to carbon in the biomass. Before entering the gasifier, the steam flow is split into two streams. One stream, containing 80% of the fed steam, enters the combustion zone (Z-2) and the other stream (20%) goes to the optimization zone (Z-4). On the other hand, oxygen is directly introduced to the combustion zone (Z-2). The char from the cyclone-1 (CL-1) is split into two streams and sent to gasification zone (Z-3) and optimization zone (Z-4). In this regard, the optimization zone (Z-4) is selected as a reference for quantifying the char split in term of mass fraction, called C to Z-4. Thus, when the entire char stream is directed to the gasification zone (Z-3), the condition is referred as C to Z-4 of 0.0.

Fig. 2 shows the molar flow rates of the major constituents of the feed and the products streams of each primary zone. It is clearly seen in Fig. 2a that the product streams contains tar, carbon and light gases including H_2, CO, CO_2, CH_4, C_2H_6, O_2, N_2 and H_2O. This result indicates that in the pyrolysis stage, the *Spirulina* biomass is completely decomposed into gaseous products and tar. The low temperature of the pyrolysis stage (973 K) favors the conversion of *Spirulina* biomass into tar

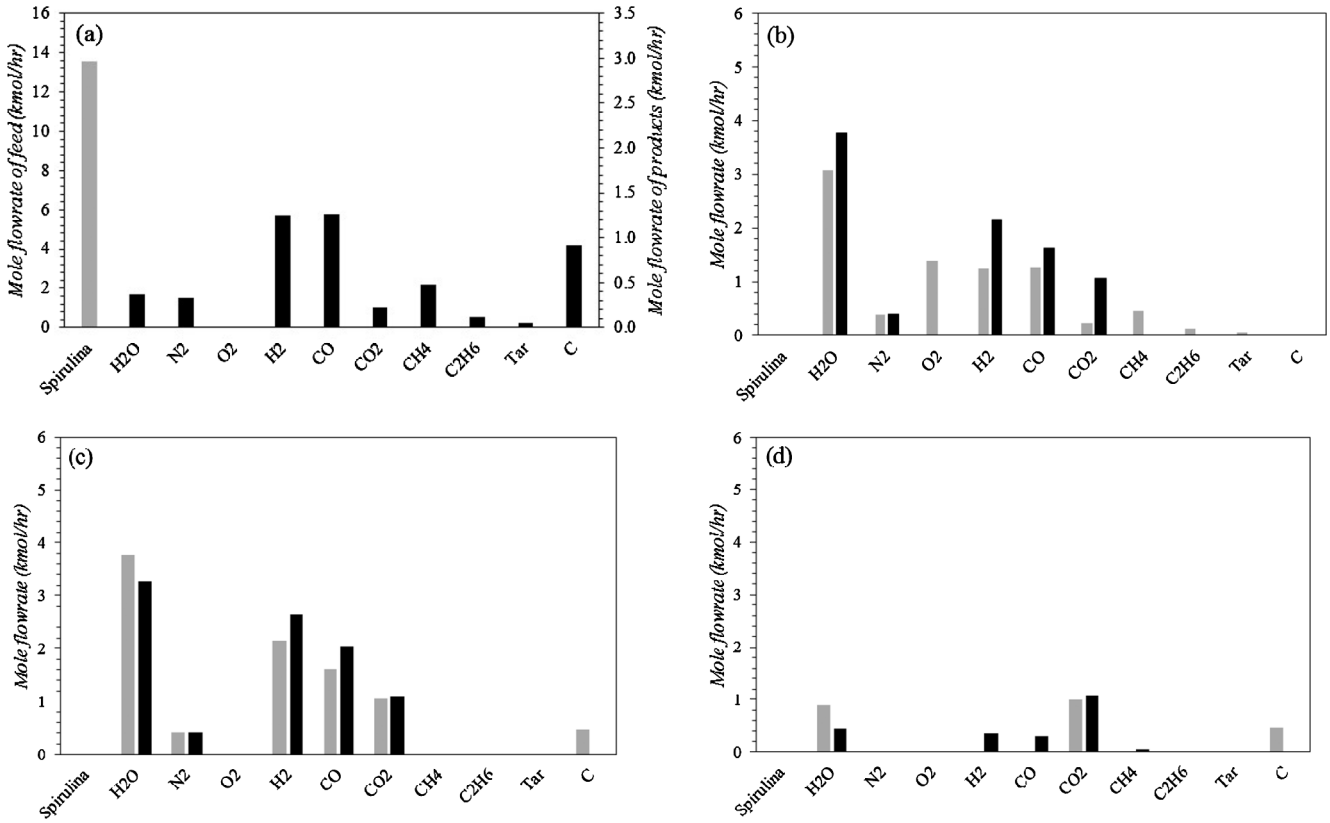

Fig. 2. Mole flow of the feed and product of (a) pyrolysis zone, (b) combustion zone, (c) gasification zone, and (d) optimization zone. (Feed: grey; product: black).

[38–40]. Following the pyrolysis step, the mixed product stream is sent to cyclone-1 (CL-1) in order to separate solids from the rest of the products. The separated solid products is sent to the splitter for splitting the char to: (1) the gasification zone (Z-3) and (2) the optimization zone (Z-4), while the gaseous products including tar are sent to the combustion zone (Z-2) for further processing.

In the combustion zone (Z-2), the gaseous pyrolysis products react with the gasifying agents (O_2 and steam) to permanent gases. As a result, the molar flow rates of CH_4, C_2H_6 and O_2 in the product stream significantly decrease, while the flow rates of H_2O and CO_2 increase (Fig. 2b). The exothermic alkane combustion reactions also increase the combustion zone temperature up to 1523 K. This high temperature facilitates the tar reforming reactions (Eqs. (7)–(10)) and converts tar into the permanent gases. This is confirmed by the absence of tar in the product stream. The tar reforming reactions also contribute to the production of H_2 and CO [30]. The combustion zone (Z-2) products flows to the gasification zone (Z-3) for further reactions.

In gasification zone (Z-3), the combustion products react with char received from the cyclone-1 (CL-1). Consequently, the carbon feed rates of the product stream decreases, while the reform products (H_2 and CO) increase, as shown in Fig. 2c. This observation indicates that the steam reforming reaction (Eq. (3)) dominates in the gasification stage. The flow rate of CO_2 in the product stream is slightly higher than its counterpart in the feed stream. This suggests the participation of the water-gas shift reaction (Eq. (4)), which is also confirmed by the decrease flow rate of H_2O. The gasification products from Z-3 is sent to the gas treatment process including Cyclone-2 (CL-2) and CO_2-absorber (AS) to remove the unconverted char and CO_2 from the main syngas stream, respectively.

In the optimization zone (Z-4), char received from the cyclone-2 (CL-2) and cyclone-1 (CL-1), reacts with pure CO_2 and steam, received from the CO_2-absorber (AS) and the boiler (BR), respectively. In Z-4, char reacts with the oxidizing agents converting C and CO_2 into CO (Eqs. (2) and (4)). This is confirmed by disappearance of carbon and increase of CO flow rates in the product stream (Fig. 2d). Interesting to see (in Fig. 2d) that the overall CO_2 flow slightly increases, despite its consumption in reaction Eq. (2). This increase of CO_2 can be explained by comparing CO_2 and H_2 production via water-gas shift reaction (Eq. (4)), which results in a higher flow rate of H_2. The slight increase of H_2 flow rate is due to hydrogen consumption in methanation reaction (Eq. (13)) to give CH_4.

6.2. The effects of O_2 equivalence ratio

The effect of O_2 equivalence ratio (ER) (varied from 0.00 to 1.00) on the gasification performance is investigated at a constant S/C ratio of 1.0. The char supplied to Z-4 is varied between 0 and 0.6 (as a fraction of total char flow) to study the effect of char split configuration at various O_2 split fractions (O_2 to Z-4 is varied between 0.0 and 0.4).

The dry basis concentrations of the primary constituents (H_2, CO and CO_2) in the syngas at various splits of char and oxygen for the O_2 ER from 0.00 to 1.00 are shown in Fig. 3. It can be clearly seen that increasing O_2 ER at a certain value favors CO_2 production and decreases the concentrations of H_2 and CO. Further increase in O_2 ER after the optimal point has minimum influence on the syngas composition. Indeed, the production of CO and H_2 is dominated by partial oxidation reaction (Eq. (1)) and steam reforming reaction (Eq. (3)). However, the presence of excessive O_2 in the gasification system promotes CO oxidation reaction (Eq. (12)), resulting in CO_2 formation and restrain the concentrations of CO and H_2. The reason for the plateau (Figs. 3a and 4a) of syngas composition at high O_2 ER can be explained by the absence of CO due to the lack of carbon source from char. The CO concentration is near to zero, where a complete carbon conversion is reached at very high O_2 ER (O_2 ER $>$ 0.92 when the C to Z-4 equals 0). Similar result is observed on the other char split fractions. These results indicate that higher amount of O_2 in the gasification process is responsible for the CO oxidation to CO_2 (Eq. (12)), leading to minimum CO production. Billdaud et al. [41] also reported similar conclusion

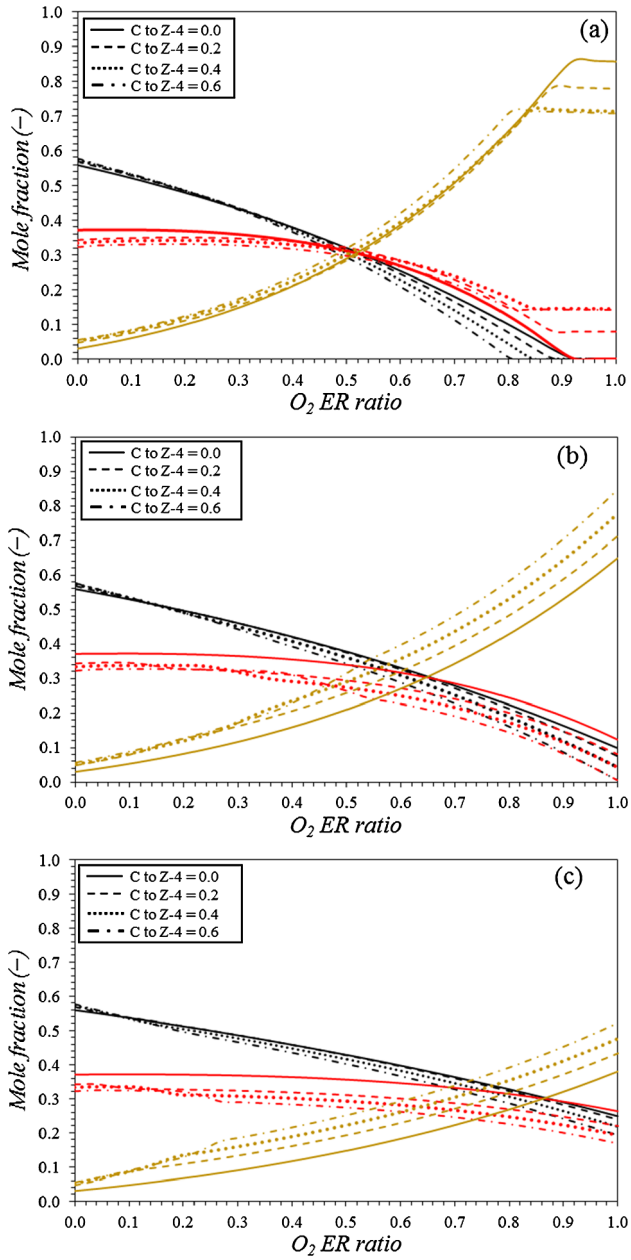

Fig. 3. The effect of O_2 equivalence ratio on the composition of syngas at different O_2 to Z-4 fractions: (a) O_2 to Z-4 of 0.0, (b) O_2 to Z-4 of 0.2 and (c) O_2 to Z-4 of 0.4. (Red: CO, black: H_2 and brown: CO_2). (For interpretation of the references to colour in this figure legend, the reader is referred to the web version of this article.)

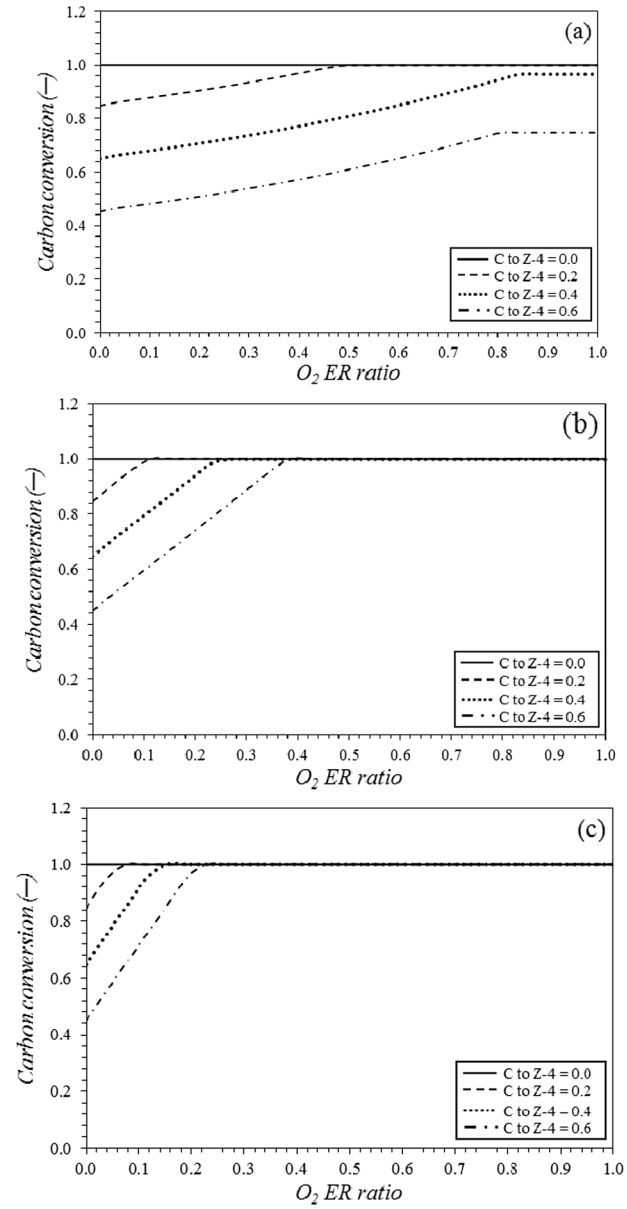

Fig. 4. The effect of O_2 ER ratio on carbon conversion at different O_2 to Z-4 fractions: (a) O_2 to Z-4 of 0.0, (b) O_2 to Z-4 of 0.2 and (c) O_2 to Z-4 of 0.4.

with a set of gasification experiments using beech wood as the feedstock. In their experiments, the highest CO concentration (24 mol/kg feedstock) was observed when O_2 ER is around 0.42. CO concentration decreased from 24 to 11 mol/kg feedstock with the increase of O_2 ER from 0.42 to 0.60.

The variation of char fed (as fraction) to Z-4 has a significant impact on the syngas composition (Fig. 4a). At high char flow and low O_2 ER, the concentrations of CO_2 and H_2 slightly increase while the concentration of CO decreases. However, the influence of char on the syngas composition fades as the O_2 ER is elevated up to a certain value. When the O_2 ER exceeds this threshold, the effect of char split becomes more prominent. The reason for this behavior comes from the fact that at this configuration O_2 is primarily sent to Z-2, which contributes to the combustion and provides high temperature and high steam H_2O concentration that facilitate the char conversion through the steam reforming reaction (Eq. (3)). At minimum char flow to the optimization zone (Z-4), the char is mainly fed to the gasification zone (Z-3), and converted into CO. It is worth noting that higher char fraction to optimization zone (Z-4) has a positive influence on CO concentration, while a negative effect is found on CO_2 concentration, especially at high O_2 ER ratio. The reason of this lays on the fact that the increase of char split to the optimization zone (Z-4) retards carbon conversion, which leads to low activity of CO combustion reaction (Eq. (12)) due to the limited CO concentration.

As mentioned above, O_2 is split into the combustion zone (Z-2) and the optimization zone (Z-4). The split fraction of O_2 to the optimization zone (Z-4) has a considerable influence on the syngas composition, by comparing Fig. 3a–c. The increase of O_2 split fraction to optimization zone (Z-4) minimizes the effect of O_2 ER ratio on the syngas composition. For example, as it can be seen in Fig. 3a that the concentration of H_2 drastically decreases from 0.58 to 0.29 with increase of O_2 ER ratio from 0.0 to 0.5 at the C to Z-4 and the O_2 to Z-4 of 0.6 and 0.0. Under similar situation, a slower reduction rate of H_2 concentration

(0.58–0.40) is observed when the O_2 to Z-4 is elevates from 0.0 to 0.4. This result indicates that the formation of syngas constituents primarily determines in the combustion zone (Z-2) and gasification zone (Z-3) due to its opportunity to receive a rich mixture of products from the pyrolysis stage (Z-1). Consequently, the presence of O_2 at higher level in the combustion zone (Z-2) has stronger control to the syngas composition given it affects the product of the gasification zone (Z-3) when compared to its counterpart in the optimization zone (Z-4), which handles a smaller number of feed compounds (mainly only char and CO_2). The identical fashion is found on the concentration of CO and CO_2.

In line with the syngas composition, the split fraction of O_2 to optimization zone (Z-4) also has a strong effect on the carbon conversions (Fig. 4). The addition of O_2 to the optimization zone (Z-4) with the O_2 to Z-4 of 0.4 slightly reduces the O_2 requirement (O_2 ER ratio of 0.08) to achieve a complete carbon conversion. This result can be explained by the fewer number of species that is involved in the optimization zone (Z-4) as compared to the species in the gasification zone (Z-2). Therefore, in the optimization zone (Z-4) the O_2 supply is exclusively reacted with char through the partial oxidation reaction (Eq. (1)). In addition, the presence of pure CO_2 from the CO_2-absorber (AS) facilitates char conversion by Bouduard reaction (Eq. (2)).

The significant influence of O_2 is also observed on the CGE, as shown in Fig. 5. It can be clearly seen in Fig. 5a that the CGE continuously decreases with the increase of O_2 ER ratio up to a certain condition in the gasification with the O_2 to Z-4 of 0.0. Further increase of O_2 supply above that O_2 ER ratio value has a negligible influence on the CGE. This result indicates that the CGE is strongly influenced by the syngas composition. The lower concentration of combustible species in the syngas due to the increase of O_2 ER ratio leads to a lower CGE. In addition, the sustained CGE with the increase of O_2 ER ratio can be related to the constant syngas composition at high O_2 ER ratio. This is confirmed by the CGE with the O_2 to Z-4 of 0.2 and 0.4 as depicted in Fig. 5b and c, respectively. Similar conclusion is previous drawn by Adnan et al. [19], reporting an adverse influence of the increase of O_2 injection to the gasification of various feedstock on the CGE.

The O_2 also has a considerable effect on the GSE, as depicted in Fig. 5. One can see in Fig. 5a that the increase of O_2 ER ratio has an adverse effect on the GSE to the minimum GSE value. Further increase of O_2 ER ratio has a negligible influence on the GSE. Again, this finding indicates that the syngas composition has a strong influence on the GSE. The similar conclusion is reported in the previous studies [19,30].

6.3. The effects of steam injection

The parametric study on the effect of steam is carried out by introducing a various boiler feed water with the S/C ratio of 0.0–2.0 at a constant *Spirulina* flow rate of 100 kg/h. In this S/C ratio parametric study, O_2 is added to the combustion zone (Z-2) at O_2 ER ratio of 0.25. The char split fraction to the optimization zone (Z-4) is varied between the C to Z-4 of 0.0 to 0.6 in order to study the effect of char at various steam split fractions to the optimization zone (Z-4) with the steam to Z-4 from 0.0 to 0.4.

Fig. 6 plots the effect of S/C ratio on dry basis syngas composition at various char and steam split fraction into the optimization zone (Z-4). It can be clearly seen from this figure that the S/C ratio significantly affects the syngas composition. The addition, steam has a positive influence on the concentration of H_2 and CO_2, while an adverse effect is found on CO concentration. This can be explained by the fact that the increase of H_2O amount in the gasification process facilitates water-gas shift reaction (Eq. (4)), consuming CO and H_2O to produce CO_2 and H_2. As per CO species, it is worth noting that the CO as a reactant of water-gas shift reaction (Eq. (4)) is produced from the conversion of carbon with the steam through reforming reaction (Eq. (3)). This is confirmed by the increase of carbon conversion with increasing S/C ratio as depicted in Fig. 7a. The present result found a good agreement with the

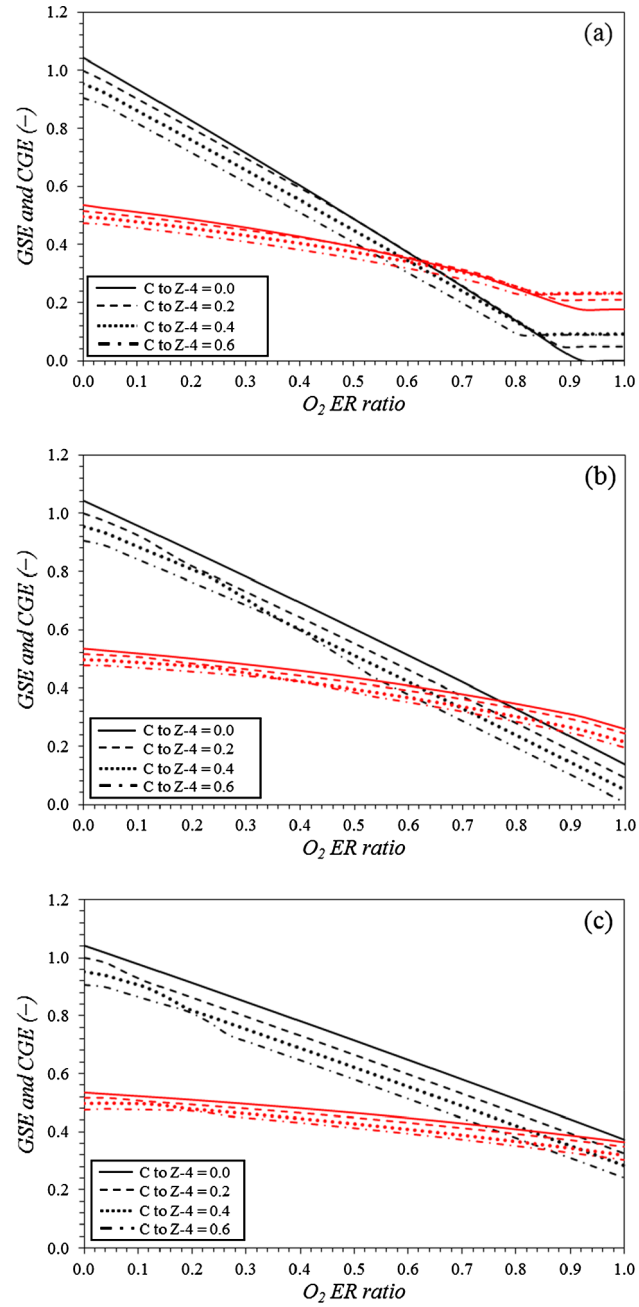

Fig. 5. The effect of equivalence ratio on GSE (red) and CGE (black) at different O_2 to Z-4 fractions: (a) O_2 to Z-4 of 0.0, (b) O_2 to Z-4 of 0.2 and (c) O_2 to Z-4 of 0.4. (For interpretation of the references to colour in this figure legend, the reader is referred to the web version of this article.)

previous experimental investigation by Li et al. [42] on the gasification using a corn stalk as the feedstock. In addition, steam contributes a considerable amount of hydrogen source for reforming reaction [43]. Similar trend is also found in the gasification with the steam to Z-4 of 0.2 and 0.4 with slight different values, as depicted in Fig. 6b and c, respectively. The char split ratio to the optimization zone (Z-4) has a minimum influence of the syngas composition. At the low S/C ratio, the concentration of CO and H_2 diminish while the CO_2 concentration elevates when the C to Z-4 is increased from 0.0 to 0.6. At high S/C ratio the opposite trend is found on the CO concentration. For instance, the CO_2 concentration slightly augments from 0.04 to 0.07 while the concentration of CO and H_2 slightly decreases from 0.41 to 0.40 and 0.49 to 0.46, respectively, when the C to Z-4 was increased from 0.0 to

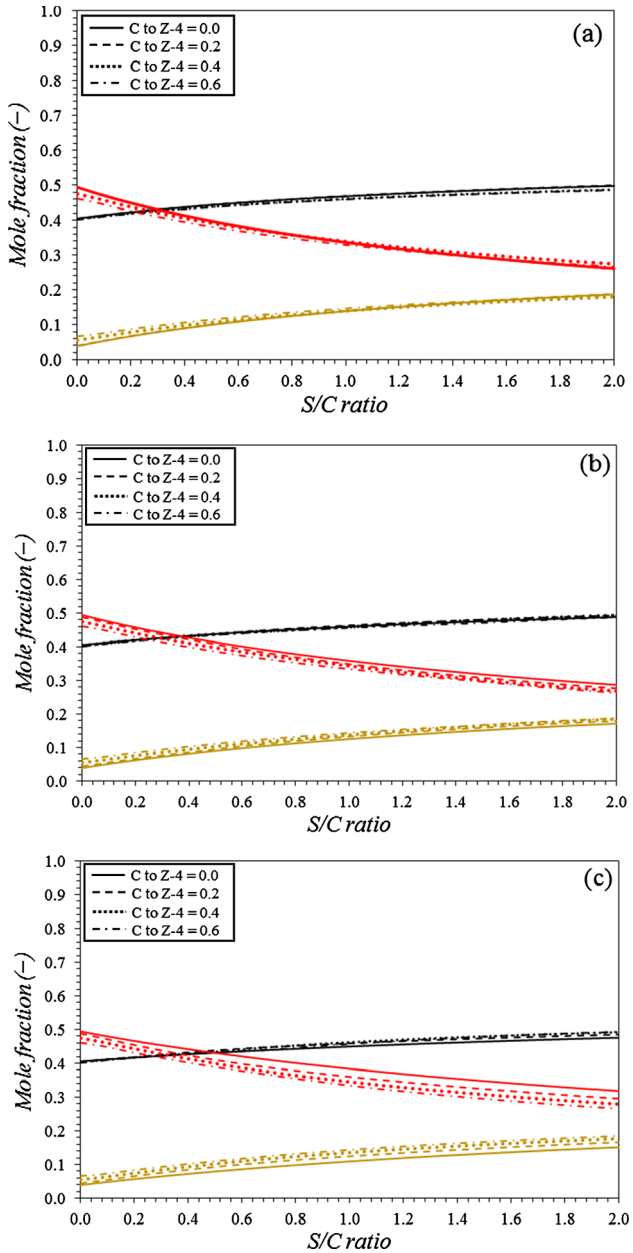

Fig. 6. The effect of S/C ratio on the composition of syngas at different steam to Z-4 fractions: (a) steam to Z-4 of 0.0, (b) steam to Z-4 of 0.2 and (c) steam to Z-4 of 0.4. (Red: CO, black: H_2 and brown: CO_2). (For interpretation of the references to colour in this figure legend, the reader is referred to the web version of this article.)

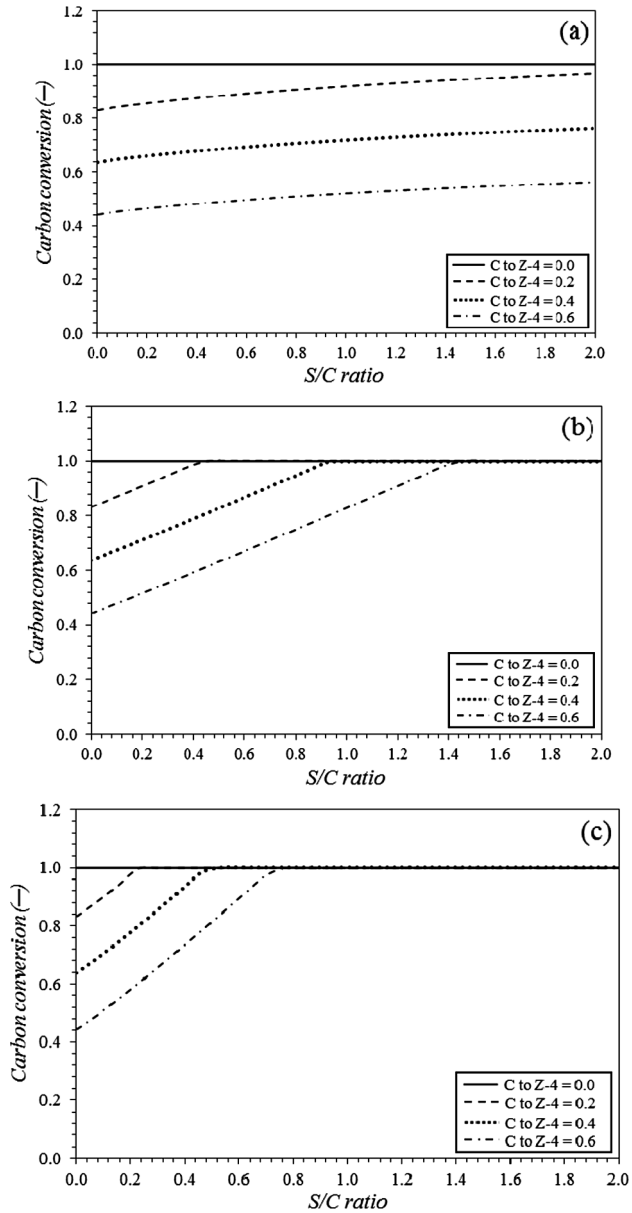

Fig. 7. The effect of S/C ratio on carbon conversion at different steam to Z-4 fractions: (a) steam to Z-4 of 0.0, (b) steam to Z-4 of 0.2 and (c) steam to Z-4 of 0.4.

0.6 on the gasification with the steam to Z-4 and the S/C ratio of 0.0 and 0.31, respectively. Under the similar conditions with higher S/C ratio (2.00), the concentration of CO slightly raises from 0.26 to 0.27 while the concentration of H_2 declined from 0.50 to 0.49 and the CO_2 concentration remains constant at 0.19. The explanation of this lays on the fact that the steam reforming reaction (Eq. (3)) has a minor influence on the syngas composition due to the small amount of char from the pyrolysis product (i.e., 10 wt%). The limited CO concentration leads to the minimum effect of the water-gas shift reaction (Eq. (4)). This is confirmed by the significant increase of carbon conversion that is not in line with the increase of CO concentration in the syngas as depicted in Figs. 7 and 6, respectively.

The influence of the char split fraction the optimization zone (Z-4) on the syngas concentration is higher when the steam split fraction to the optimization zone (Z-4) is increased from 0.0 to 0.4, as shown in Fig. 6a–c. This can be explained by the fact that the steam reforming reaction (Eq. (3)), which is promoted by steam injection, facilitates conversion of carbon and steam into CO and H_2. It is worth noting that at higher steam to Z-4, the domination of the water-gas shift (Eq. (4)) reaction increases due to the excess amount of steam, converting CO and steam into CO_2 and H_2.

The considerable effect of steam at various char split fraction to the optimization zone (Z-4) is also found on the CGE, as depicted in Fig. 8. The CGE slightly mitigates with the increase of S/C ratio from 0.0 to 2.0 at the C to Z-4 of 0.0. These results can be explained by the fact that the increase of heating value due to the slight increase of H_2 concentration is counterbalanced by the significant decrease of CO concentration, resulting a decline of net syngas heating value. This is an indication of strong influence of syngas composition on the CGE. The similar fashion is observed on the gasification with the steam to Z-4 of 0.2 and 0.4, as shown in Fig. 8b and c, respectively. The identical conclusion is reported in the previous published literature [19]. The char split fraction to the optimization zone (Z-4) has a negative effect on the CGE at low

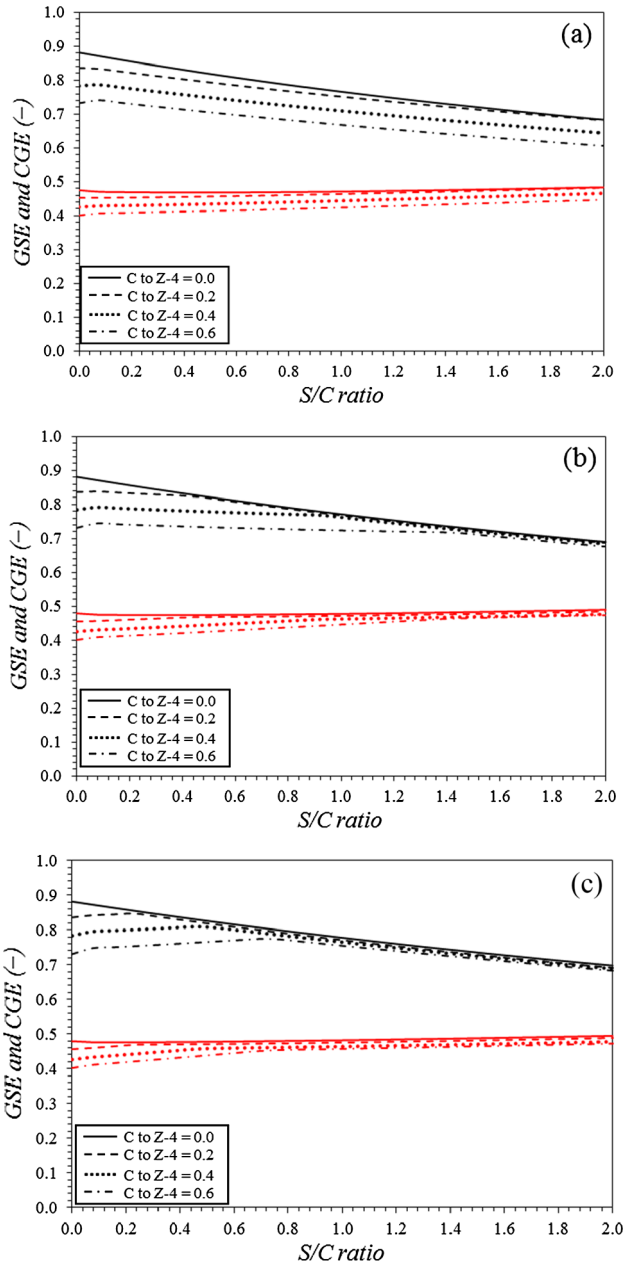

Fig. 8. The effect of S/C ratio on GSE (red lines) and CGE (blak lines) at different steam to Z-4 fractions: (a) steam to Z-4 of 0.0, (b) steam to Z-4 of 0.2 and (c) steam to Z-4 of 0.4.

S/C ratio. The influence of the char split fraction diminishes at higher S/C ratios. This indicates that lower carbon conversion results in lower CGE due to the reduction of syngas flow rate. This is confirmed by the decrease of carbon conversion at higher C to Z-4, as depicted in Fig. 7.

The steam also has a positive influence on the GSE, as shown in Fig. 7. One can see from this figure that the GSE slightly increases from 0.47 to 0.48 with the increase of S/C ratio from 0.0 to 2.0 for the gasification with C to Z-4 and C to Z-4 of 0.0 and 0.0, respectively (Fig. 7a). The higher increase of GSE is observed on higher char split fraction to the optimization zone (Z-4). For instance, on the gasification at the C to Z-4 of 0.6, the GSE significantly elevates from 0.40 to 0.45 with the increase of S/C ratio from 0.0 to 2.0 for steam to Z-4 of 0.0. The identical fashion is observed on the steam to Z-4 of 0.2 and 0.4 as depicted in Fig. 7b and c, respectively. This indicates that the addition of steam facilitates an exothermic CO combustion reaction (12) given the steam promotes steam reforming reactions (Eq. (3)) which produce CO. This is confirmed by the increase of CO_2 concentration as the S/C ratio is elevated, as depicted in Fig. 6.

7. Conclusions

A new biomass gasification configuration is developed using Aspen Plus software, considering the formation of tar during the pyrolysis stage. The *Spirulina* microalgae is considered as the biomass feedstock. Following are the conclusion of this study:

i. The performances (syngas composition, cold gas efficiency and gasification system efficiency) of gasification process vary with different char, O_2 and steam split fraction to the optimization zone (Z-4).
ii. The use of suitable amount of oxygen (O_2 ER) as a gasifying agent enables a complete reforming of tar into syngas in the combustion zone (Z-2).
iii. The use of steam as a gasifying agent facilitates H_2 production. The highest H_2 concentration (0.58) is observed on the gasification at O_2 ER ratio and S/C ratio of 0.0 and 1.0, respectively, for char to Z-4 and O_2 to Z-4 of 0.6 and 0.0, respectively.
iv. The highest CGE (1.04) and GSE (0.52) is found in gasification at the O_2 ER ratio, the S/C ratio and C to Z-4 of 0.0, 1.0, 0.0, respectively for all studied O_2 to Z-4 (0.0, 0.2, and 0.4).
v. The inclusion of the optimization zone (Z-4) promotes the concentration of CO and H_2 at the controlled use of gasifying agents.

Acknowledgements

The author(s) would like to acknowledge the financial support provided by the Deanship of Scientific Research (DSR) at King Fahd University of Petroleum & Minerals (KFUPM) for funding this work through project No. IN161022. We also would like to acknowledge the supports from the directorate of research and community services at Islamic University of Indonesia (DPPM-UII).

References

[1] de Lasa H, Salaices E, Mazumder J, Lucky R. Catalytic steam gasification of biomass: catalysts, thermodynamics and kinetics. Chem Rev 2011;111:5404.
[2] Nautiyal P, Subramanian KA, Dastidar MG. Production and characterization of biodiesel from algae. Fuel Process Technol 2014;120:79.
[3] Adnan MA, Hossain MM. CO_2 gasification of microalgae (N. Oculata) – a thermodynamic study. MATEC Web Conf 2018;154:01002.
[4] Adnan MA, Hossain MM. Co-gasification of Indonesian coal and microalgae – a thermodynamic study and performance evaluation. Chem Eng Process - Process Intensif 2018;128:1.
[5] Slade R, Bauen A. Micro-algae cultivation for biofuels: cost, energy balance, environmental impacts and future prospects. Biomass Bioenergy 2013;53:29.
[6] Park H, Lee C-G. Theoretical calculations on the feasibility of microalgal biofuels: utilization of marine resources could help realizing the potential of microalgae. Biotechnol J 2016;11:1461.
[7] Richardson JW, Johnson MD, Lacey R, Oyler J, Capareda S. Harvesting and extraction technology contributions to algae biofuels economic viability. Algal Res 2014;5:70.
[8] Valderrama Rios ML, González AM, Lora EES, Almazán del Olmo OA. Reduction of tar generated during biomass gasification: a review. Biomass Bioenergy 2018;108:345.
[9] Jia S, Ning S, Ying H, Sun Y, Xu W, Yin H. High quality syngas production from catalytic gasification of woodchip char. Energy Convers Manage 2017;151:457.
[10] Anis S, Zainal ZA. Tar reduction in biomass producer gas via mechanical, catalytic and thermal methods: a review. Renew Sust Energ Rev 2011;15:2355.
[11] Guan G, Kaewpanha M, Hao X, Abudula A. Catalytic steam reforming of biomass tar: Prospects and challenges. Renew Sust Energy Rev 2016;58:450.
[12] Fagbemi L, Khezami L, Capart R. Pyrolysis products from different biomasses: application to the thermal cracking of tar. Appl Energy 2001;69:293.
[13] Jiang L, Liu C, Hu S, Wang Y, Xu K, Su S, et al. Catalytic behaviors of alkali metal salt involved in homogeneous volatile and heterogeneous char reforming in steam gasification of cellulose. Energy Convers Manage 2018;158:147.
[14] Abu El-Rub Z, Bramer EA, Brem G. Review of catalysts for tar elimination in biomass gasification processes. Ind Eng Chem Res 2004;43:6911.
[15] Mazumder J, De Lasa H. Fluidizable Ni/La2O3-γAl2O3 catalyst for steam gasification of a cellulosic biomass surrogate. Appl Catal B 2014;160–161:67.
[16] Adnan MA, Muraza O, Razzak SA, Hossain MM, de Lasa HI. Iron oxide over silica-

doped alumina catalyst for catalytic steam reforming of toluene as a surrogate tar biomass species. Energy Fuels 2017;31(7):7471–81.
[17] Susanto H, Beenackers AACM. A moving-bed gasifier with internal recycle of pyrolysis gas. Fuel 1996;75:1339.
[18] Brandt P, Larsen E, Henriksen U. High tar reduction in a two-stage gasifier. Energy Fuels 2000;14:816.
[19] Adnan MA, Hossain MM. Gasification performance of various microalgae biomass – a thermodynamic study by considering tar formation using Aspen plus. Energy Convers Manage 2018;165:783.
[20] Tang Y, Liu J. Effect of anode and Boudouard reaction catalysts on the performance of direct carbon solid oxide fuel cells. Int J Hydrogen Energy 2010;35:11188.
[21] Masmoudi MA, Halouani K, Sahraoui M. Comprehensive experimental investigation and numerical modeling of the combined partial oxidation-gasification zone in a pilot downdraft air-blown gasifier. Energy Convers Manage 2017;144:34.
[22] Adnan MA, Hossain MM. Gasification of various biomasses including microalgae using CO_2 – a thermodynamic study. Renew Energy 2018;119:598.
[23] Adnan MA, Susanto H, Binous H, Muraza O, Hossain MM. Feed compositions and gasification potential of several biomasses including a microalgae: a thermodynamic modeling approach. Int J Hydrogen Energy 2017;42:17009.
[24] Fortunato B, Brunetti G, Camporeale SM, Torresi M, Fornarelli F. Thermodynamic model of a downdraft gasifier. Energy Convers Manage 2017;140:281.
[25] Han J, Liang Y, Hu J, Qin L, Street J, Lu Y, et al. Modeling downdraft biomass gasification process by restricting chemical reaction equilibrium with Aspen Plus. Energy Convers Manage 2017;153:641.
[26] Xiang X, Gong G, Shi Y, Cai Y, Wang C. Thermodynamic modeling and analysis of a serial composite process for biomass and coal co-gasification. Renew Sust Energ Rev 2018;82:2768.
[27] Zhang X, Li H, Liu L, Bai C, Wang S, Zeng J, et al. Thermodynamic and economic analysis of biomass partial gasification process. Appl Therm Eng 2018;129:410.
[28] Gopaul SG, Dutta A, Clemmer R. Chemical looping gasification for hydrogen production: a comparison of two unique processes simulated using ASPEN Plus. Int J Hydrogen Energy 2014;39:5804.
[29] Mostafavi E, Pauls JH, Lim CJ, Mahinpey N. Simulation of high-temperature steam-only gasification of woody biomass with dry-sorption CO_2 capture. Can J Chem Eng 2016;94:1648.
[30] Adnan MA, Susanto H, Binous H, Muraza O, Hossain MM. Enhancement of hydrogen production in a modified moving bed downdraft gasifier – a thermodynamic study by including tar. Int J Hydrogen Energy 2017;42:10971.
[31] Hong Y, Chen W, Luo X, Pang C, Lester E, Wu T. Microwave-enhanced pyrolysis of macroalgae and microalgae for syngas production. Bioresour Technol 2017;237:47.
[32] Renganathan T, Yadav MV, Pushpavanam S, Voolapalli RK, Cho YS. CO_2 utilization for gasification of carbonaceous feedstocks: a thermodynamic analysis. Chem Eng Sci 2012;83:159.
[33] Yan L, He B. On a clean power generation system with the co-gasification of biomass and coal in a quadruple fluidized bed gasifier. Bioresour Technol 2017;235:113.
[34] Fagbemi L, Khezami L, Capart R. Pyrolysis products from different biomasses. Appl Energy 2001;69:293.
[35] Benson SW, Cruickshank FR, Golden DM, Haugen GR, O'Neal HE, Rodgers AS, et al. Additivity rules for the estimation of thermochemical properties. Chem Rev 1969;69:279.
[36] Tijmensen MJA, Faaij APC, Hamelinck CN, van Hardeveld MRM. Exploration of the possibilities for production of Fischer Tropsch liquids and power via biomass gasification. Biomass Bioenergy 2002;23:129.
[37] Peters L, Hussain A, Follmann M, Melin T, Hägg MB. CO2 removal from natural gas by employing amine absorption and membrane technology—a technical and economical analysis. Chem Eng J 2011;172:952.
[38] Duman G, Uddin MA, Yanik J. Hydrogen production from algal biomass via steam gasification. Bioresour Technol 2014;166:24.
[39] Stark AK, Bates RB, Zhao Z, Ghoniem AF. Prediction and validation of major gas and tar species from a reactor network model of air-blown fluidized bed biomass gasification. Energy Fuels 2015;29:2437.
[40] Stark AK, Ghoniem AF. Quantification of the influence of particle diameter on Polycyclic Aromatic Hydrocarbon (PAH) formation in fluidized bed biomass pyrolysis. Fuel 2017;206:276.
[41] Billaud J, Valin S, Peyrot M, Salvador S. Influence of H_2O, CO_2 and O_2 addition on biomass gasification in entrained flow reactor conditions: experiments and modelling. Fuel 2016;166:166.
[42] Li B, Yang H, Wei L, Shao J, Wang X, Chen H. Hydrogen production from agricultural biomass wastes gasification in a fluidized bed with calcium oxide enhancing. Int J Hydrogen Energy 2017;42:4832.
[43] Shayan E, Zare V, Mirzaee I. Hydrogen production from biomass gasification; a theoretical comparison of using different gasification agents. Energy Convers Manage 2018;159:30.

ScienceDirect

Fuel

Supports *open access*

11.2	8.035
CiteScore	Impact Factor

Submit your article | Guide for authors

Menu Search in this journal

Latest issue

Volume 345

In progress • 1 August 2023

About the journal

The Science and Technology of Fuel and Energy

Research into **energy sources** remains a key issue. Over the last 90 years, Fuel has been the leading source of primary research work in **fuel science**. The scope is broad and includes many topics of increasing interest such as environmental aspects and pollution.

A wide variety of fuels are covered:
•…

View full aims & scope

6.5 weeks
Review Time

1.8 weeks
Publication Time

View all insights

Principal Editors | View full Editorial Board

FEEDBACK

Articles

Latest published | Articles in press | Top cited | Most downloaded | Most popular

Review article Full text access

Synthesis, characterization and electrochemical aspects of graphene based advanced supercapacitor electrodes

B.B. Sahoo, ... M.K. Nayak

1 August 2023

View PDF

Research article Full text access

Simulation of mercury distribution in an offshore natural gas processing platform

Vassilis Koulocheris, ... Epaminondas Voutsas

1 August 2023

View PDF

Research article Full text access

Synthesis of cardanol grafted hydrophilic polymers and its mechanism of coal dust inhibition

Zhilin Xi, ... Lianquan Suo

1 August 2023

View PDF

Research article Full text access

Bio-inspired mineralization of CO_2 into $CaCO_3$: Single-step carbon capture and utilization with controlled crystallization

Dharmjeet Madhav, ... Veerle Vandeginste

1 August 2023

View PDF

Research article *Open access*

Computational study of the multidimensional spread of smouldering combustion at different peat conditions

Han Yuan, ... Guillermo Rein

1 August 2023

View PDF

Research article Full text access

Selective hydrogenation of oleic acid over Flower-like Ni-Fe/SiO_2-ZrO_2 catalyst to produce fatty alcohol: Effect of SiO_2

Fei Wang, ... Jianchun Jiang

1 August 2023

View PDF

Research article Full text access

Molecular dynamics simulations of the nickel removal from crude oil by neutral and charged spherical polymer brushes

Kaili Shen, ... Jun Xu

1 August 2023

View PDF

Research article Full text access

Experimental study on the effect of piston bowl geometry on the combustion performance and pollutant emissions of methane-diesel common rail dual-fuel engine

Halil Erdi Gulcan, Murat Ciniviz

1 August 2023

View PDF

Read latest issue

Calls for papers

Towards Cleaner Production of Greener Fuels for Future & Sustainable Energy Systems, Green Production and Sustainable Energy-ICAFEE 2023

Guest editors: Abdulaziz ATABANI, Fares ALMOMANI, Amani AL-OTHMAN, Kyu-Jung CHAE - Submission deadline: 5 April 2024

This Special Issue at FUEL will contain peer-reviewed and high-quality papers selected from The 6th International Conference on Alternative Fuels, Energy and Environment: Future & Challenges (ICAFEE 2023). The conference will be held in October …

Recent advances in green ammonia production and storage (GAPS)

Guest editors: Sabarathinam Shanmugam, Giovanni Cinti, Jiao Xue Submission deadline: 30 October 2023

Carbon-neutral fuels came to the limelight to circumvent the staggering energy crisis issue of the world population. Of the different carbon-free fuels proposed, ammonia stands out as one of the promising fuels owing to its global mass production, …

The 17th International Conference on Stability, Handling and Use of Liquid Fuels

Guest editors: Matthew DeWitt; Jinxia Fu; Simon Blakey Submission deadline: 31 March 2023

The International Association on Stability, Handling and Use of Liquid Fuels (IASH) is the foremost international organization devoted to all aspects of the stability, handling, and use of liquid fuels from refinery to end use. The mission of IASH …

View all calls for papers for special issues

Special issues and article collections

Fuels, Combustion, Engines and Fire Conference & Combustion Symposium 2020

Edited by Hakan Serhad Soyhan, Nafiz Kahraman, Gökhan Coşkun, Üsame Demir

17 March 2023

28th International Conference on the Impact of Fuel Quality on Power Production and the Environment

Edited by Flemming J. Frandsen, Stanley Harding, Terry Wall, Markus Broström, Maria Zevenhoven

17 February 2023

The 17th International Conference on Stability, Handling and Use of Liquid Fuels

Edited by Matthew DeWitt, Jinxia Fu, Simon Blakey, Bastian Rauch

1 December 2022

Reaction engineering during biomass gasification

Edited by Lu Ding, Guangsuo Yu, Fuchen Wang, Benyamin Khoshnevisan

28 November 2022

View all special issues and article collections

View all issues

Partner journals

Fuel Communications

Open access

Related journals

Fuel Communications

Fuel Communications

Print ISSN: 0016-2361
Online ISSN: 1873-7153

For Authors

Track your accepted paper

Journal Finder

Researcher Academy

Rights and permissions

Journal Article Publishing Support Center

For Editors

Publishing Ethics Resource Kit

Guest Editors

For Reviewers

Reviewer recognition

FUEL

the science and technology
of Fuel and Energy

Fuel

Supports *open access*

11.2 CiteScore | 8.035 Impact Factor

Volume 241

Pages 1-1236 (1 April 2019)

Previous vol/issue | Next vol/issue

Full text access

Editorial Board

Page ii

View PDF

Reviews

Review article Full text access

Recent advances of surfactant-stabilized N_2/CO_2 foams in enhanced oil recovery

Lin Sun, Baojun Bai, Bing Wei, Wanfen Pu, ... Changyong Zhang

Pages 83-93

View PDF Article preview

Abstract

Abstract

Foam has been applied in enhanced oil recovery (EOR) for more than sixty years. The surfactant-stabilized N_2/CO_2 foams are two of the most widely used foams in foam EOR processes, and numerous oil reservoirs could potentially benefit from them. This paper comprehensively reviews the development of these foams over the past decade. We focused on the promising surfactant formulas and their corresponding mechanisms under different reservoir conditions, especially harsh conditions. The most recent

studies have shown that low interfacial tension foaming surfactants are efficient in fractured/tight reservoirs, while CO_2-switchable surfactants are well suited to CO_2 foam in carbonate reservoirs with high temperatures. Pure surfactants and mixed surfactants that combine anions and cations contain superior foam properties. The surfactant aggregates, such as vesicles and wormlike micelles, could distinctly enhance the foam stability. However, the adsorption of the mixed surfactants on reservoir

Review article Full text access

Formation, transformation, measurement, and control of SO_3 in coal-fired power plants

Chenghang Zheng, Yifan Wang, Yong Liu, Zhengda Yang, ... Xiang Gao
Pages 327-346

View PDF Article preview

Abstract

Abstract

The formation and emission of sulfur trioxide (SO_3) in coal-fired power plants has received increasing attention due to its adverse effects on the operation of plant and environment. With the wide application of selective catalytic reduction (SCR) systems, the problem caused by SO_3 has become severe, especially when high sulfur coal is burned. Emission regulations of SO_3 for coal-fired power plants, which promote the development of SO_3 measurement and control technologies, have been set in some countries and regions. In this paper, recent advances in the formation, transformation, measurement, and control mechanism and technologies of SO_3 in coal-fired power plants were summarized. The formation mechanisms of SO_3 in boiler and SCR systems and its form transition and corresponding effects on the performance of power plants were analyzed. Different SO_3 test standards and methods were compared, and online SO_3 monitor based on isopropanol absorption method were developed. Various SO_3 control technologies, including simultaneous and specific removal technology, were summarized. Low-low temperature and wet

Research article Full text access

On the molecular basis of aggregation and stability of Colombian asphaltenes and their subfractions

Lina R. Morantes, Ana M. Percebom, Enrique Mejía-Ospino
Pages 542-549

View PDF Article preview

Abstract

Abstract

Vacuum residue (VR) is the heaviest fraction obtained by fractional distillation of the crude oil. Crude oil and its fractions, such as VR, can be separated in its components saturates, aromatics, resins, and asphaltenes (SARA fractions). Asphaltenes are of particular importance for up- and down-stream processes due to their molecular complexity, high heteroatom content, and strong tendency to self-aggregate. To evaluate the molecular characteristics of asphaltenes responsible for aggregation, we used a fractionation method based on mixtures of toluene and acetone to separate asphaltenes, isolated from a heavy Colombian residue, into different solubility subfractions. In this contribution, we show correlations between elemental composition and average molecular properties of subfractions and their solubility behavior. In addition, we were able to differentiate asphaltenes into 'unstable' and 'stable' subfractions in toluene solution by an analytical centrifugation method. From the stability analysis, we demonstrated that less soluble subfractions (consisting of more aromatic, heavier, and more condensed asphaltenes) are more

Review article Full text access

A comprehensive review on interaction of nanoparticles with low salinity water and surfactant for enhanced oil recovery in sandstone and carbonate reservoirs

Saheed Olawale Olayiwola, Morteza Dejam
Pages 1045-1057

View PDF Article preview

Abstract

Abstract

Nanoparticles (NPs) are currently gaining wide acceptance in the field of petroleum engineering. They are applied in different areas of petroleum exploration and production such as drilling, well logging, reservoir management, and enhanced oil recovery (EOR). Due to the size of NPs, they have special physical and chemical properties. Therefore, NPs can influence the properties of the fluid system, including viscosity, magnetism, and interfacial tension (IFT).

The injection of NPs into the reservoirs for EOR is more effective than water injection but not as effective as chemical flooding. Consequently, NPs are injected along with low salinity water (LSW) or chemicals such as surfactant in order to improve the recovery of oil. NPs are used to prevent the fines migration during LSW injection, control the mobility of formation water, and reduce the surfactant adsorption on the pore walls of the reservoir.

Full Length Articles

Research article Full text access

Rapid fabrication of $KTa_{0.75}Nb_{0.25}/g\text{-}C_3N_4$ composite via microwave heating for efficient photocatalytic H_2 evolution

Zhiqiang Chen, Pengfei Chen, Pingxing Xing, Xin Hu, ... Yiming He
Pages 1-11

View PDF Article preview

Abstract Graphical abstract

Graphical abstract

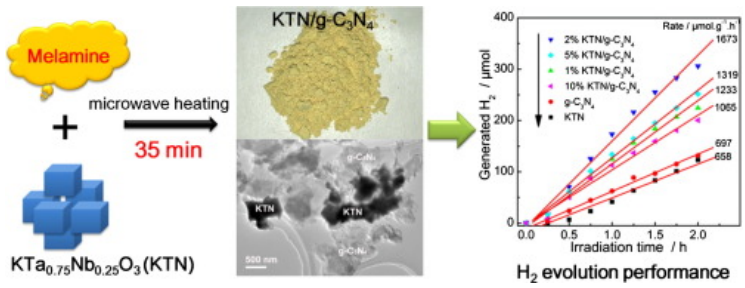

Research article Full text access

Investigation of gas slippage effect and matrix compaction effect on shale gas production evaluation and hydraulic fracturing design based on experiment and reservoir simulation

Courtney Rubin, Mehrdad Zamirian, Ali Takbiri-Borujeni, Ming Gu
Pages 12-24

View PDF Article preview

Abstract

Abstract

Recent core-lab study of Marcellus Shale illustrated that effect of gas slippage and matrix compaction are significant on gas production because of substantial reservoir pressure depletion, especially during the late time of gas production. However, the impact of gas slippage and matrix compaction on gas recovery evaluation and hydraulic fracturing design is still not clearly understood and systematically investigated. Additionally, such impact varies with production time and completion/production circumstances. Therefore, it is critical to develop a laboratory-modeling based approach that properly characterizes the two permeability effects and evaluates their impact on well production evaluation and hydraulic fracturing design.

In this study, a comprehensive parametric study is conducted by running reservoir simulations using empirical permeability correlations developed from core-lab tests under different confining stress and pore pressure conditions. Simulations of different

Research article Full text access

Effect of residual air bubbles on diesel spray structure at the start of injection

M. Ghiji, L. Goldsworthy, V. Garaniya, P.A. Brandner, ... P. Joseph

Pages 25-32

View PDF Article preview

Abstract

Abstract

Experimental and numerical analyses of the effect of residual air bubbles in a single-hole high-pressure diesel injector nozzle are presented. Detailed information on spray structures and dynamics near nozzle exit at the Start of Injection (SOI) is described. Experimental measurements are performed using a laser-based backlit imaging technique through a long distance microscope by injecting diesel fuel into a constant volume high-pressure spray chamber. Numerical investigation of, in and near-nozzle fluid dynamics is conducted in an Eulerian framework using a Volume of Fluid (VOF) interface capturing technique integrated with Large Eddy Simulation (LES) turbulence modelling. The present flow setup includes residual air bubbles remaining from a previous injection event, in-nozzle turbulence with no-slip wall conditions. Experimental images show a toroidal starting vortex near the nozzle exit suggesting a partially filled nozzle; transparency in the emerging jet demonstrates the presence of air trapped inside the nozzle liquid from the previous injection event. The numerical model provides insight into the influence of residual air

Research article Full text access

Experimental investigations of wall jet droplet impact on spray impingement fuel film formation

Hujie Pan, Di Xiao, David Hung, Min Xu, Xuesong Li

Pages 33-41

View PDF Article preview

Abstract

Abstract

The understanding of fuel spray impingement phenomenon and its impact of film formation on wall are significant for engine related applications, such as emission reduction and lubrication improvement, etc. However, the impingement phenomenon of the airborne droplets in the wall jet moving parallel to the wall has not been fully understood yet, especially for the fact that

negligible amount of fuel film is formed underneath the wall jet. In this experimental research, various laser diagnostic techniques, including laser-induced fluorescence, Mie scattering, phase Doppler interferometry, and particle imaging velocimetry were utilized to capture both macroscopic and microscopic behavior of the spray impingement process. It was found that droplets in the spray with a high tangential velocity may be governed by the lift force induced by the boundary layer near the plate, gliding away without impinging the wall and forming wall film. Based on the observations, a modified impingement criterion is proposed

Research article Full text access

Investigation of electrical properties with medium and heavy Brazilian crude oils by electrochemical impedance spectroscopy

John W.S. Rocha, Maristela A. Vicente, Breno N. Melo, Maria de Lourdes S.P. Marques, ... Maria F.P. Santos
Pages 42-52

View PDF Article preview

Abstract Graphical abstract

Graphical abstract

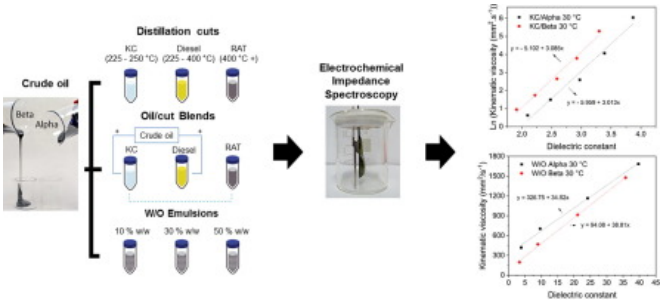

Research article Full text access

A new model of emulsion flow in porous media for conformance control

Long Yu, Boxin Ding, Mingzhe Dong, Qi Jiang
Pages 53-64

View PDF Article preview

Abstract

Abstract

Emulsion flow in porous media is of paramount importance to the use of emulsions in the conformance control and enhanced oil recovery processes. In this paper, a new theoretical model, incorporating physical properties of porous media, physicochemical properties of the emulsion system, injection strategy, and the interactions between porous media and emulsion, was developed to quantitatively describe flow behaviors of emulsions in porous media. The resistance factor of an emulsion when transported in porous media was first derived through a-two phase flow method. The strong interaction between emulsion droplets and porous media was characterized by the capillary resistance force in the model. A non-uniform capillary model which considers size differences of the pore-body and pore-throat in porous media was proposed to represent the complicated real porous media. By analyzing the adsorption and plugging properties of different emulsion droplets in the non-uniform capillary model, the capillary resistance force was finally determined. To describe emulsion flow in the subsequent water flooding process after emulsion

Research article Full text access

Improving biodiesel monoglyceride determination by ASTM method D6584-17

Teresa L. Alleman, Earl D. Christensen, Bryan R. Moser
Pages 65-70

View PDF Article preview

Abstract

Abstract

Biodiesels produced from commercial and non-traditional feedstocks were analyzed by ASTM D6584-17 for monoglyceride (monoacylglycerol, or MG) content. It was found that D6584-17 as currently written may not accurately determine MGs from conventional feedstocks due to significant differences in retention time using modern instrumentation. For biodiesel from non-traditional feedstocks, D6584-17 did not sufficiently account for MGs containing fatty acids outside of C16 and C18 species. This led to under- and over-reporting of MGs, as critical components were not accurately measured. Improvements to the method were made through a three-step process. First, a standard mixture of MGs was run to determine the retention time of individual MGs that could be present in the samples from C10 to C24. An additional analysis for the fatty acid methyl ester (FAME) profile was used to determine the major MG species present in the biodiesel samples, using the assumption that the MG profile was proportional to the FAME profile. The biodiesel samples were analyzed by D6584-17, and the MGs were identified using

Research article Full text access

Impact of gasoline direct injection fuel injector hole geometry on spray characteristics under flash boiling and ambient conditions

Changzhao Jiang, Matthew C. Parker, Jerome Helie, Adrian Spencer, ... Graham Wigley
Pages 71-82

View PDF Article preview

Abstract

Abstract

The effect of injector nozzle design on the Gasoline Direct Injection (GDI) fuel spray characteristics under atmospheric and flash boiling conditions was investigated using Phase Doppler Anemometry (PDA) measurements. To understand the impact of hole diameter and conicity, experiments were conducted on two bespoke 3-hole injectors in a pressure and temperature controlled constant volume chamber and in the open air. The measurements were taken radially outward from the injector axis to the outer extent of the plume at distances of 15 mm, 25 mm and 40 mm from the injector tip.

Observations of the influence of surrounding gas and temperature conditions and hole design on the injector spray performance were made. Under non-flash boiling conditions, it was found that the injection pressure dictates the length of the spray penetration before collapse occurs, with an increase in pressure resulting in an increase in this length. Comparison of mean

Research article Full text access

Effects analysis on the gasification kinetic characteristics of food waste in supercritical water

Jingwei Chen, Yi Fan, Jiaqiang E, Wen Cao, ... Wenwen Xu
Pages 94-104

View PDF Article preview

Abstract Graphical abstract

Graphical abstract

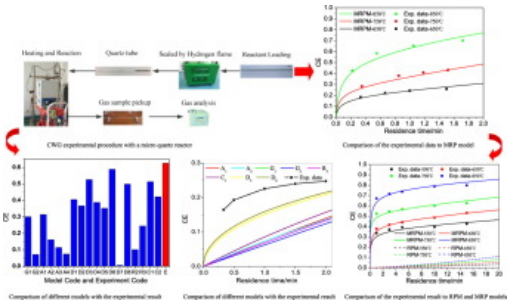

Research article Full text access

Intrinsic relationship between Langmuir sorption volume and pressure for coal: Experimental and thermodynamic modeling study

Yun Yang, Shimin Liu, Wei Zhao, Liang Wang
Pages 105-117

View PDF Article preview

Abstract

Abstract

Gas adsorption volume has long been recognized as an important parameter for coalbed methane (CBM) resource assessment as it determines the overall gas capacity of coal. As the industrial standard practice, Langmuir volume (V_L) is used to describe the gas adsorption volume. Another important parameter, Langmuir pressure (P_L), is typically overlooked because it does not directly relate to the resource estimation. However, P_L defines the slope of the adsorption isotherm and the ability of a well to attain the critical desorption pressure in a significant reservoir volume, which is critical to plan the initial water depletion rate for a CBM well. Qualitatively, both V_L and P_L are related to the fractal pore structure of coal, but the intrinsic relationships among fractal pore structure, V_L, and P_L are not well studied and quantified due to the complex pore structure of coal. In this study, a series of experiments were conducted to measure the fractal dimensions of coal and their relationship to methane adsorption capacity. The thermodynamic model of the gas adsorption on heterogonous surfaces was revisited, and the theoretical models

Research article Full text access

System simulation and experimental verification: Biomass-based integrated gasification combined cycle (BIGCC) coupling with chemical looping gasification (CLG) for power generation

Huijun Ge, Haifeng Zhang, Wanjun Guo, Tao Song, Laihong Shen
Pages 118-128

View PDF Article preview

Abstract

Abstract

Biomass-based integrated gasification combined cycle (BIGCC) is a power generation technology to convert biomass fuel to electricity. In view of biomass gasification characteristic, chemical looping gasification (CLG) is an innovative biomass utilization technology. Due to the presence of metal oxygen carrier materials in CLG process, syngas yield can be increased and tar catalytic cracking is occurred. In this paper, a new system integrating BIGCC with CLG is designed for power generation and the simulation of the whole process, including biomass gasification, gas cleaning, heat recovery steam generator (HRSG) and

gas/steam turbine, are carried out with Aspen Plus software. At first, in order to ensure the model accuracy, the experiments in a 25 kW_{th} reactor of interconnected fluidized beds are conducted and the experiment results are compared with the simulated results from the designed model. It is verified that the designed biomass gasification model, especially kinetic model and

Research article Full text access

Effect of reflux digestion time on MoO_3/ZrO_2 catalyst for sulfur-resistant CO methanation

Jia Gu, Zhong Xin, Miao Tao, Yuhao Lv, ... Qian Si
Pages 129-137

View PDF Article preview

Abstract Graphical abstract

Graphical abstract

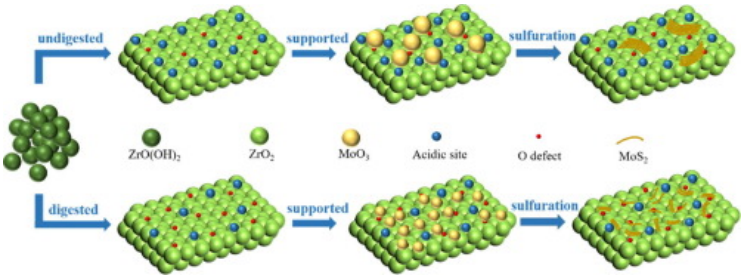

Research article Full text access

Experimental study on soot formation, evolution and characteristics of diffusion ethylene/air flames in ψ-shaped mesoscale combustors

Mingfei Chen, Dong Liu, Yaoyao Ying, Kai Lei, ... Bo Jiang
Pages 138-154

View PDF Article preview

Abstract Graphical abstract

Graphical abstract

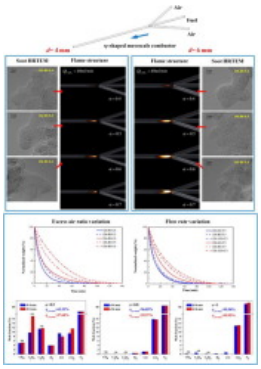

Research article *Open access*

Ultrasonic parameter measurement as a means of assessing the quality of biodiesel production

Raphaela M. Baêsso, Rodrigo P.B. Costa-Felix, Piero Miloro, Bajram Zeqiri
Pages 155-163

View PDF Article preview

Abstract Graphical abstract

Graphical abstract

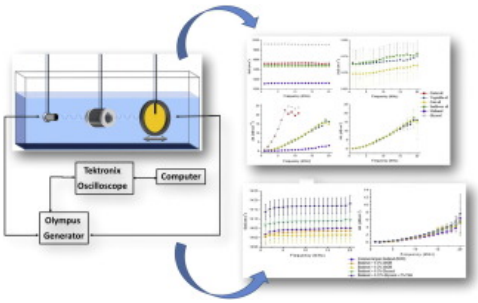

Research article Full text access

The stage evolution characteristics of gas transport during mine gas extraction: Its application in borehole layout for improving gas production

Leilei Si, Zenghua Li, Yongliang Yang, Ruiting Gao
Pages 164-175

View PDF Article preview

Abstract

Abstract

Diffusion and seepage play a significant role in the mine gas extraction, while their influence degree is dynamic with the change of time or location, showing a notable dynamic stage characteristic. Therefore, it is significant to master the conversion node of gas transport for improving the gas production. However, it is difficult to determine the conversion node and master controlling roles during mine gas extraction due to the lack of judgment index. In this work, a dual-porosity model was constructed to describe the gas transport in coal seam. Then, a transfer coefficient ratio between gas diffusion and gas seepage was used to define as the conversion node. Furthermore, our model was validated by comparing with the previous model, showing that our model can better describe the evolution of gas pressure under different stress conditions. The influence of stress, initial permeability and initial diffusion coefficient on the conversion node were investigated. Results showed that the initial permeability shows the most notable influence on the conversion node, followed by the stress. The initial diffusion coefficient has

Research article Full text access

Combustion of straight algae oil in a swirl-stabilized burner using a novel twin-fluid injector

Oladapo S. Akinyemi, Lulin Jiang, Rafael Hernandez, Carl McIntyre, Williams Holmes
Pages 176-187

View PDF Article preview

Abstract

Abstract

The current study investigates the combustion performance of straight algae oil (AO) in a 7-kW lab-scale gas turbine burner enabled by a novel twin-fluid injector, named Swirl-burst (SB) injector. The chemical structure (fatty acid profile), the physical, and chemical properties of AO are acquired to understand the combustibility of the oil as a potential biofuel. Effects of

equivalence ratio (ER) and atomizing air to liquid mass ratio (ALR) across the injector on the global combustion characteristics are investigated at a constant heat release rate for the oil. The features of interest include visual flame images, product gas temperature, emissions of carbon monoxide (CO), and nitrogen oxides (NOx) at the combustor exit. Results show that mono-unsaturated fatty acid is predominant in the composition of the oil, suggesting possibly short ignition delay. AO has a heating value comparable to that of diesel but with a high kinematic viscosity (approximately 16 times more viscous than diesel). Clean

Research article Full text access

Raman spectroscopic study of chemical structure and thermal maturity of vitrinite from a suite of Australia coals

Yulong Zhang, Zhongsheng Li

Pages 188-198

View PDF Article preview

Abstract

Abstract

The deconvolution and resolution of overlapping bands in the Raman spectra of a suite of coals studied by curve-fitting methods has improved our understanding of the main structural changes in naturally matured coals. Even though much work on deconvolution of Raman spectra has been done, the systematic evolution of chemical structures is not well established. In this study we used a suite of 28 coal samples from Australia with vitrinite reflectance ranging from 0.38 to 3.52%. The micro-Raman spectra of vitrinite macerals from selected coals were acquired using a custom-made Raman spectrometer and supplemented by other Raman spectra previously acquired under the same experimental conditions. In the spectral deconvolution procedure, the second derivative curve-fitting method was used to determine the number of peaks and peak positions of the Raman spectra. Each band was tentatively assigned to a corresponding chemical structure by references to the interpreted major structural changes likely to have taken place during coalification. These parameters included P_D (the position of D band), RBS (the distance

Research article Full text access

Evolution of volatile cloud in pulverized coal combustion with high-speed digital inline holographic visualization

Xiaodan Lin, Yingchun Wu, Chenyue Wu, Longchao Yao, ... Kefa Cen

Pages 199-206

View PDF Article preview

Abstract

Abstract

The coal devolatilization plays a significant role in the combustion of pulverized coal particles. The evolution of volatile cloud during devolatilization of pulverized coal particles (105–125 μm) is studied in a high-temperature flat-flame burner by combining high-speed photography with high-speed digital inline holography (DIH). By the high-speed holographic visualization, the evolution of volatile cloud of pulverized coal from volatile release to soot aggregation generation can be divided into four stages. Effects of coal type on volatile cloud evolution are investigated using three different coals, i.e., Shanxi bituminous coal, Ximeng lignite and Yinni lignite. The results show that both the Shanxi bituminous coal and Ximeng lignite produce soot aggregation during devolatilization, which is rarely observed for Yinni lignite. Moreover, Shanxi bituminous coal has a higher potential in soot cluster formation for its higher coal rank than Ximeng lignite. The high-speed reconstructed image sequences are analyzed to measure the velocity slip between the parent particle and volatile cloud. Compared with Shanxi bituminous coal, Ximeng

Research article Full text access

Efficient upgrading of pyrolysis bio-oil over Ni-based catalysts in supercritical ethanol

Jin-Hyuk Lee, In-Gu Lee, Ji-Yeon Park, Kwan-Young Lee
Pages 207-217

View PDF Article preview

Abstract Graphical abstract

Graphical abstract

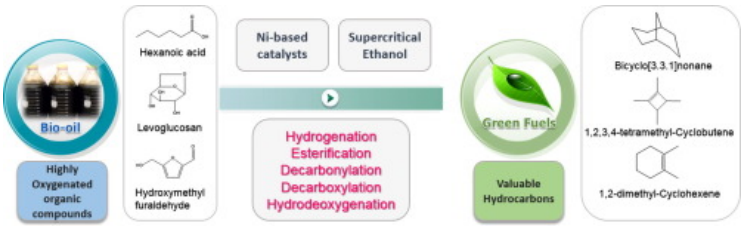

Research article Full text access

Viscosity of oxygenated fuel: A model based on Eyring's absolute rate theory

Chenyang Zhu, Feng Yang, Xiangyang Liu, Waheed Afzal, Maogang He
Pages 218-226

View PDF Article preview

Abstract

Abstract

A viscosity model was proposed for oxygenated fuel components; it was based on Eyring's absolute rate theory and a cubic equation of state Soave-Redlich-Kwong. The viscosity was associated with flow energy which could be divided into the activation energy and the vacancy-formation energy, and then a reference state for simplifying the calculation process was introduced in the present model. This work also reported a viscosity database at temperatures from 243.15 K to 413.15 K and pressures up to 200 MPa for 31 oxygenated fuel components containing alcohols, esters and ethers in order to verify the proposed model. The average absolute relative deviations between calculated and experimental data were lower than 2.37%. Furthermore, the free-volume model, which has a similar consideration of flow energy with this work, was chosen to further investigate the performance of the present model, and in general, the present model showed a better accuracy than the free-volume model. Finally, it was shown that the proposed model could be extended to the mixtures successfully.

Research article Full text access

Characterizing particulate matter emissions in an aviation kerosene-fueled model combustor at elevated pressures and temperatures

Chi Zhang, Xiaotong Mi, Xin Hui, Longfei Chen, ... Chih-Jen Sung
Pages 227-233

View PDF Article preview

Abstract

Abstract

The present study investigated the characteristics of particulate matter (PM) emissions in a single-dome, Rich-Quench-Lean, model combustor under different operating conditions typical for aero-engines, with special emphasis on identifying the individual effects of pressure, temperature, and equivalence ratio on PM emissions in aero-combustors. Results showed that the number-based particle size distribution was shifted from the nucleation mode (<50 nm) to the accumulation mode (50–1000 nm) as the dome equivalence ratio increased from 0.944 to 1.267. When the dome equivalence ratio further increased from 1.342 to 1.814, the number distribution was shifted to smaller particle sizes that are dominated by the nucleation mode. With the increase of operating pressure, the PM emissions have a notably higher number concentration with smaller size particles. While

Research article Full text access

Petroleum generation kinetic models for Late Ordovician kukersite Yeoman Formation source rocks, Williston Basin (southern Saskatchewan), Canada

Zhuoheng Chen, Xiaojun Liu, Kirk G. Osadetz

Pages 234-246

View PDF Article preview

Abstract

Abstract

Ordovician Yeoman Fm. kukersite source rocks from Canadian Williston Basin are composed almost exclusively of *Gloeocapsomorpha prisca (G. prisca)* alginite. Thermocatalytic petroleum generation from *G. prisca* alginite differs significantly from that of amorphous bituminite typical of marine Type II source rocks. Commonly used petroleum generation kinetic parameter optimization procedures that assume n^{th} order chemical reactions fail to reproduce sample Flame Ionization Detector (FID) pyrograms using expected chemical bond activation energies. A parallel nucleation-growth reaction model (PN-GRM) successfully addresses these deficiencies for this specific kerogen type. Programed pyrolysis of seventeen kukersite sample FID pyrograms as well as two additional kukersite Rock-Eval datasets reveal the kinetic characteristics of this globally significant, but stratigraphically restricted marine Type I source rock. The results show that the PN-GRM closely approximates the chemical reactions as demonstrated by reproduction of kukersite FID pyrograms, that kukersite source rocks are thermally more stable as

Research article Full text access

Assessment of the performance of asphaltene inhibitors using a multi-section packed bed column

Jun Kuang, Ariana A. Melendez-Alvarez, Josiah Yarbrough, Miguel Garcia-Bermudes, ... Francisco M. Vargas

Pages 247-254

View PDF Article preview

Abstract

Abstract

Asphaltene deposition is one of the major problems in the production, transportation, and processing of crude oils. The precipitated and subsequently deposited asphaltenes could cause the plugging of production tubing, significantly reducing oilfield productivity. Conventional asphaltene dispersants, particular types of asphaltene deposition inhibitors, are chemical supposedly used to improve the stability of oils, thereby preventing asphaltene deposition in the oilfield pipelines. The Asphaltene Dispersion Test (ADT) and the Solid Detection System (SDS) have been used to assess the performance of the asphaltene deposition inhibitors; however, these techniques have several limitations caused by the conceptual understanding of the asphaltene deposition mechanism and the instrument detection limit. Thus, the conventional asphaltene dispersants assessed by the ADT and the SDS might provide misleading results on the effectiveness of these chemicals to mitigate asphaltene deposition. The conventional asphaltene dispersants are developed based on their ability to reduce the size of asphaltene

Research article Full text access

Insights into the high-temperature oxidation of methylcyclohexane

Yalan Liu, Guangyue Li, Junxia Ding
Pages 273-282

View PDF Article preview

Abstract

Abstract

Reactive molecular dynamics simulations were performed under different conditions in order to investigate in-detail the chemical events associated with high-temperature oxidation of methylcyclohexane (MCH). The corresponding kinetic behaviors of the major intermediates and products were systematically analyzed at the atomistic level. Thus the overall reaction scheme of MCH oxidation was established from the initial step to the final products. It was observed that the oxidation of MCH was mainly initiated by two kinds of reactions, including unimolecular decomposition and H abstraction, with the former being more important. In agreement with the available experimental results, C_2H_4, CH_2O, CO, CO_2 and H_2O were found to be the major products during the oxidation process. The results revealed that $\cdot CH_3O_2$, $\cdot CH_3O$ and $\cdot C_3H_5O$ radicals were the precursors for CH_2O production, which was the key intermediate to generate CO. Additionally, $\cdot C_2H_3O$ also had closed relationship with the formation of CO. For a better description of the combustion behavior, small oxides related to intermolecular reactions should be

Research article Full text access

Study on the generation of active sites during low-temperature pyrolysis of coal and its influence on coal spontaneous combustion

Jinhu Li, Zenghua Li, Yongliang Yang, Xiaoyan Zhang
Pages 283-296

View PDF Article preview

Abstract Graphical abstract

Graphical abstract

The thermal decomposition of oxygen-containing functional groups in coal will generate active sites, and the exothermic oxidation of active sites at room temperature is the initial source of heat for spontaneous combustion of the pyrolyzed coal.

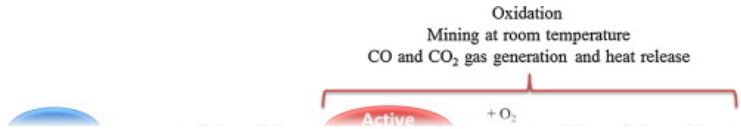

Research article Full text access

Asphalt as raw material of graphene-like resources

Salvador Fernández, Alfonso Mercado, Edgar Cuara, Claudia Yeverino-Miranda, Uriel Sierra
Pages 297-303

View PDF Article preview

Abstract

Abstract

In search of alternate procedures and raw materials to manufacture graphene oxide and graphene derivatives that could be scaled up to be industrially implemented, we have developed a simple thermal treatment of petroleum asphalt that gives rise to graphite oxide-like materials in high yield. Subsequent treatment of the oxide at higher temperature gives rise to graphene-like products similar to those obtained by conventional top-down methods based on graphite. The method offers economy in manufacturing time and energy spent, allowing the valorization of a waste material.

Research article Full text access

Prediction of ash-deformation temperature based on grey-wolf algorithm and support-vector machine

Haiping Xiao, Yuhui Chen, Chaozong Dou, Yu Ru, ... Baomin Sun
Pages 304-310

View PDF Article preview

Abstract

Abstract

To explore the effect of sulfate on the ash-fusion temperature (AFT) of coal ash, different contents of calcium sulfate were added to coal ash, and AFT and X-ray diffractometry (XRD) spectral analyses were carried out. The AFT of experimental coal ash was reduced at a low content, but when the calcium sulfate ($CaSO_4$) content increased beyond 15%, the coal-ash AFT increased. The deformation temperature of real coal ash was predicted based on the content of different components and a combination of the coal-ash parameters. The support-vector machine model was optimized by using the grey-wolf algorithm. The model could predict the deformation temperatures of the different coal ash and a more accurate prediction model was obtained. In the grey-wolf-algorithm-support-vector-machine model, 58 coal samples were used, and SO_3 was compared as an independent variable for training prediction. The results showed that the relative error of the deformation-temperature prediction was small and the prediction result with the SO_3 input was more accurate, which agrees with the experimental results.

Research article Full text access

Biodiesel production from heterogeneous catalysts based K_2CO_3 supported on extruded γ-Al_2O_3

Euripedes G. Silveira Junior, Victor Haber Perez, Inés Reyero, Ana Serrano-Lotina, Oselys Rodriguez Justo
Pages 311-318

View PDF Article preview

Abstract Graphical abstract

Graphical abstract

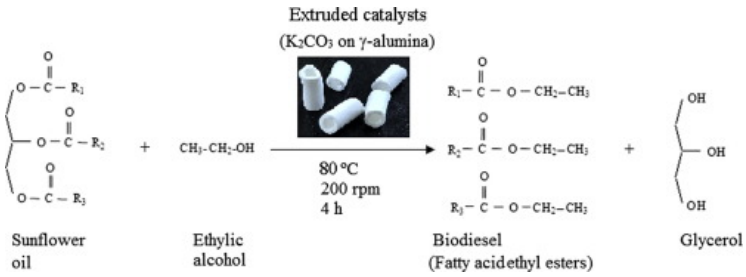

Research article Full text access

A new method of estimating derived cetane number for hydrocarbon fuels

Yu Wang, Yi Cao, Wei Wei, David F. Davidson, Ronald K. Hanson
Pages 319-326

View PDF Article preview

Abstract

Abstract

A new spectroscopic predictor for estimating ignition characteristics including derived cetane number is proposed for hydrocarbon fuels. This spectroscopic predictor is the ratio of room temperature absorbance of unreacted fuel vapor at 3.41 and 3.39 μm, termed here as the "3.41/3.39 absorption ratio." Its wide availability and applicability are demonstrated for a range of pure hydrocarbons, mixtures of pure hydrocarbons, and distillate and synthetic jet fuels. Quasi-linear calculation methods are provided for practical use. Spectroscopic and kinetic interpretations are provided based on the fraction of $-CH_2-$ hydrogen relative to all carbon-bonded hydrogen. In addition, the correlations between the proposed predictor and ignition delay time and C_2H_4 yield are presented and discussed to exhibit the predictor's potential as a fuel screening tool.

Research article Full text access

A new method of geochemical allocation and monitoring of commingled crude oil production using trace and ultra-trace multi-element analyses

Weihang Yang, John F. Casey, Yongjun Gao, Jiaxuan Li
Pages 347-359

View PDF Article preview

Abstract

Abstract

Production allocation refers to the practice of quantifying proportions of extracted commingled hydrocarbons across various contributing sources. In this paper we tested a new geochemical technique of trace element production allocation by analyzing the mass fractions of specific target elements in five end-member natural crude oils and the manually mixed crude oil in precisely controlled proportions. We analyzed target elements by ICP-OES and Triple Quadrupole (QQQ)-ICP-MS techniques in tandem

on each sample. In our test, the contributing fractions of the five end-member oils were measured by weight and mixed in proportions of ~30%, 25%, 20%, 15%, and 10% in the commingled oil. The obtained mass fractions for specific target elements in both the five end-member oils and the commingled oil are input into a program developed called "ALLO-TRACE". ALLO-TRACE calculates the contributing fractions of all the end-member oils to the commingled oil using multiple analyte-based linear

Research article Full text access

Characterizations of pore, mineral and petrographic properties of marine shale using multiple techniques and their implications on gas storage capability for Sichuan Longmaxi gas shale field in China

Hao Xu, Wen Zhou, Rui Zhang, Shimin Liu, Qiumei Zhou
Pages 360-371

View PDF Article preview

Abstract

Abstract

Pore, mineral and petrographic properties of shale conjunctionally determine the gas storage and transport properties of gas shale reservoirs. To investigate how these characteristics and pore structure influence the methane adsorption capability of shale formation, a total of forty-nine over-matured shale outcrop samples, thirty samples from Upper Longmaxi Formation and nineteen samples from Lower Longmaxi Formation from southern Sichuan Basin in China, were collected. Multiple techniques, including geochemical and mineralogical measurements, field emission-scanning electron microscopy (FE-SEM), mercury intrusion porosimetry (MIP), low-pressure CO_2 and N_2 adsorption and high-pressure methane adsorption, were employed to characterize the geo-properties, pore structure and their impacts on methane adsorption capacity under different temperatures. Geochemical and mineralogical results show that both Upper and Lower Longmaxi shales are over-matured which have oil-prone type I kerogen. Based on the FE-SEM observation, most of the organic matter (OM) pores in the tested Longmaxi shales are

Research article Full text access

Gasification performance of *Spirulina* microalgae – A thermodynamic study with tar formation

Muflih A. Adnan, Qingang Xiong, Arif Hidayat, Mohammad M. Hossain
Pages 372-381

View PDF Article preview

Abstract

Abstract

In this work, the performance of a novel configuration for *Spirulina* microalgae gasification was investigated through an improved thermodynamic model using Aspen Plus. Compared with existing thermodynamic models, tar formation is included in the improved counterpart. The proposed novel gasification process consists of four primary zones: (i) pyrolysis, (ii) combustion, (iii) gasification, and (iv) optimization. First, the modeling results were compared against experimental values, where a good agreement (relative error < 10%) was obtained under identical operating conditions. Then, performance of the novel gasification configuration was studied using the developed improved thermodynamic model at various operating conditions. Metrics such as gasification system efficiency, syngas composition and cold gas efficiency were used to measure the performance. It was found that incorporation of the optimization zone improves the concentration of CO and H_2 at the controlled use of gasifying agents. Moreover, injection of suitable amount of gasifying agents enhances the gasification performance. Finally, the effects of O

Research article Full text access

Kinetic analysis and modeling of coal pyrolysis with model-free methods

Jingchong Yan, Hanren Jiao, Zhanku Li, Zhiping Lei, ... Chunxiu Pan
Pages 382-391

View PDF Article preview

Abstract

Abstract

Knowledge about the rate of coal pyrolysis is of great importance because it exerts remarkable effect on its thermal conversions such as combustion, gasification and liquefaction. Different approaches can be used to obtain the kinetics of coal pyrolysis, the simplest are empirical and global kinetics, where Arrhenius expression is used to correlate the mass loss with temperature. This work conducted pyrolysis of a lignite and a bituminite at various heating rates with a thermo-gravimetric analyzer (TGA). Thermogravimetry coupled with mass spectroscopy (TG-MS), solid state ^{13}C Cross Polarization/ Magic Angle Spinning nuclear magnetic resonance (^{13}C CP/MAS NMR) and Raman analyses were also conducted to correlate the structural characteristics and pyrolysis behavior of the coals. Kinetic analysis was performed by using three model-free methods including Distributed Activation Energy model (DAEM), Ozawa-Flynn-Wall (OFW) and Friedman method. Kinetic modeling was also performed based on the DAEM model with multiple Gaussian sub-distributions of activation energy. The results show that DAEM, OFW and

Research article Full text access

Analysis of light weight fractions of coal-based crude oil by gas chromatography combined with mass spectroscopy and flame ionization detection

Wen-ying Li, Wei Wang, Hai Mu, Wang Li, ... Jie Feng
Pages 392-401

View PDF Article preview

Abstract Graphical abstract

Graphical abstract

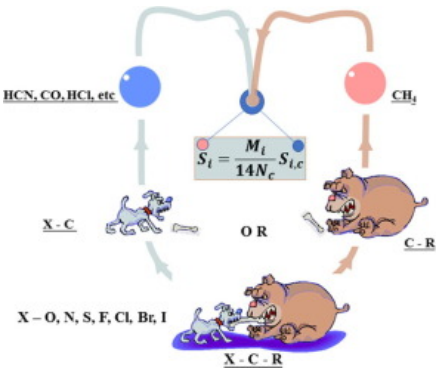

Research article Full text access

A semi-empirical NO_x model for LES in pulverized coal air-staged combustion

Zhi Zhang, Yuxin Wu, Denggao Chen, Haoshu Shen, ... Benjamin J. Isaac
Pages 402-409

View PDF Article preview

Abstract

Abstract

Numerical simulation of pulverized coal combustion with the large eddy simulation (LES) method can provides important instructions on the design optimization of boilers. Because of its huge computational cost, a simple but reliable NO_x prediction model is required in LES. Through the air-staged combustion experiments of six kinds of coals which conducted in an electric heated down-fired furnace (DFF), the relationship between NO_x reduction and $CO + H_2$ generation in the fuel-rich zone was identified. Based on this observation, a semi-empirical modeling strategy was proposed: instead of CH_i which is difficult to calculate, the concentration of $CO + H_2$ is used to quantify NO homogeneous reduction. An integrated NO_x prediction model was proposed and implemented into LES simulation. The results proved the new model can accurately predict different NO_x evolution characteristics under various conditions. Furthermore, the comparison indicated the LES method performs better on NO_x prediction than the RANS method, especially in the area where the turbulent fluctuation is relatively stronger.

Research article Full text access

Direct estimation of shale oil potential by the structural insight of Indian origin kerogen

Veena R. Bansal, Ravindra Kumar, M.I.S. Sastry, R.M. Badhe, ... Deepak Saxena

Pages 410-416

View PDF Article preview

Abstract

Abstract

Structural insight of Indian origin kerogen has been investigated by Solid State ^{13}C Cross Polarization Magic Angle Spinning Nuclear Magnetic Resonance (^{13}C CPMAS NMR) and Infrared (IR) Spectroscopic techniques. Cross Polarization (CP) with decoupling using two pulse phase modulation (TPPM) and Bloch decay experiment with 1H decoupling have been performed on each kerogen sample. Direct estimation of oil potential present in Indian origin kerogen has been done utilizing developed method based on IR and ^{13}C CPMAS NMR techniques. The IR methods have been developed using both transmission and DRIFT reflectance spectra by employing standard blends of oil shale (1–12%) with Vacuum Gas Oil (VGO) range products. Models were developed by correlating the IR intensity in 3000–2700 cm^{-1} region with the % oil shale in VGO. Validation has been done by estimating aliphatic carbon (C_{alip}) and aromatic carbon (C_{arom}) content obtained by ^{13}C CPMAS NMR method and a comparison has been made between ^{13}CMAS NMR with and without dipolar dephasing, with and without CP. ^{13}C MAS NMR spectra of Indian

Research article Full text access

Fate of sulfur in chemical looping combustion of gaseous fuels using a Perovskite oxygen carrier

Robert F. Pachler, Stefan Penthor, Karl Mayer, Hermann Hofbauer

Pages 432-441

View PDF Article preview

Abstract

Abstract

In the present study, the influence of sulfuric fuel impurities on CLC is investigated in a 120 kW_{th} chemical looping combustion pilot unit consisting of two interconnected circulating fluidized beds. An in industrial scale produced perovskite type $CaMn_{0,775}Mg_{0,1}Ti_{0,125}O_{3-\delta}$, called C28 has been used as oxygen carrier. The oxygen carrier is manufactured by spray drying method. As fuel natural gas from the grid, originally without sulfur, is used. To investigate the influence of sulfur, H_2S has been added to the fuel stream up to a concentration of 3000 ppmv. The measurements have been performed at operating temperatures of 950 °C. For closing the mass balance of sulfur, the exhaust gas streams of air and fuel reactor are analyzed against H_2S and

SO_2. To investigate potential interaction of sulfur with the particles, SEM, ICP-OES, XRF and XRD analysis have been carried out with solid samples of the oxygen carrier particles.

Research article Full text access

Study on the regenerable sulfur-resistant sorbent for mercury removal from nonferrous metal smelting flue gas

Zongwen Quan, Wenjun Huang, Yong Liao, Wei Liu, ... Zan Qu
Pages 451-458

View PDF Article preview

Abstract Graphical abstract

Graphical abstract

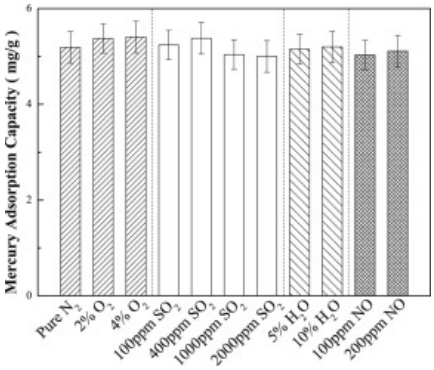

Research article Full text access

Identification of CO_2 sequestration opportunities: CO_2 miscible flooding guidelines

Na Zhang, Mingfei Yin, Mingzhen Wei, Baojun Bai
Pages 459-467

View PDF Article preview

Abstract

Abstract

Carbon dioxide (CO_2) flooding has been demonstrated as an economically feasible technique for carbon capture and storage (CCS) via enhanced oil recovery (EOR). In the oil industry, most of the CO_2-EOR projects were implemented in miscible phase (CO_2 miscible flooding), and it has become the most productive EOR method in the United States since 2012. Successful implementation of CO_2 miscible flooding requires comprehensive guidelines about where CO_2 can be applied. With the development of new technology, the suitable conditions for CO_2-EOR have changed. Therefore, updating the guidelines for CO_2-EOR is necessary. In this study, we updated the guidelines for field CO_2 miscible applications in the United States by collecting valuable information from about 100 publications. Significant parameters for CO_2 miscible flooding such as minimum miscibility pressure (MMP) and pay zone net thickness were considered for the first time in comparison with existing research studies. After data processing/cleaning, 207 projects have remained in the dataset. Combination plots were created to explore the ranges

Research article Full text access

Combustion, vibration and noise analysis of hydrogen-diesel dual fuelled engine

Sarthak Nag, Priybrat Sharma, Arpan Gupta, Atul Dhar
Pages 488-494

View PDF Article preview

Abstract

Abstract

The transportation sector of the present-day world is facing severe problems like increasing global pollution and continuous depletion of conventional energy resources; both at alarming rates; which has motivated the researchers to look for alternative fuels and study various aspects of clean burning and sustainable fuels. The vibration of the engines during the combustion is one crucial aspect, as it defines the overall ride quality and comfort of an automobile. In this work, the authors have studied dual fuel combustion using a constant speed diesel engine, operated using hydrogen and diesel. The experimental studies are carried at the load of 25%, 50% and 75% with the substitution of diesel with hydrogen for the energy share of 0%, 5%, 10% and 20%. The effect of hydrogen addition on the combustion characteristics, vibrations and acoustics in the engine is investigated. In this study, marginal pernicious effects of hydrogen addition on the in-cylinder pressure are observed, particularly at lower loads. However, the vibration and noise level sees a reduction with hydrogen addition. The effect of combustion characteristics on noise and

Research article Full text access

Comparison of hydrocracking kinetic models based on SARA fractions obtained in slurry-phase reactor

Guillermo Félix, Jorge Ancheyta

Pages 495-505

View PDF Article preview

Abstract Graphical abstract

Graphical abstract

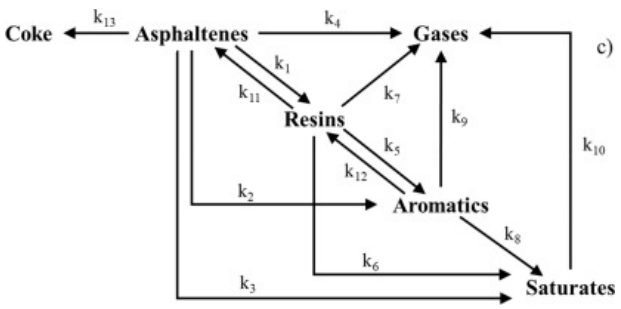

Research article Full text access

Single-cylinder engine evaluation of a multi-component Diesel surrogate fuel at partially-premixed and low-temperature combustion modes

Patrick G. Szymkowicz, Jesús Benajes

Pages 506-518

View PDF Article preview

Abstract

Abstract

To investigate and develop efficient and clean combustion systems, advanced CFD modeling tools need accurate kinetic models capable of predicting the chemical and physical processes that take place in the combustion chamber during and after fuel injection and air mixing. Given the complex composition of market Diesel fuels, simpler surrogate fuels composed of a limited

number of pure substances are used to model the physical, chemical, and combustion properties of Diesel fuel. The surrogates must closely reproduce the market Diesel fuel properties and duplicate the real-world engine combustion and emissions behavior. Previous work created a multi-component surrogate fuel that consisted of normal-hexadecane/2,2,4,4,6,8,8-heptamethylnonane/decahydronaphthalene/1-methylnaphthalene. The surrogate fuel properties closely matched the market Diesel fuel. The surrogate fuel was then evaluated under conventional Diesel engine combustion conditions and obtained

Research article Full text access

Pyrolytic behavior of coal-related model compounds connected with C–C bridged linkages by in-situ pyrolysis vacuum ultraviolet photoionization mass spectrometry

Yang Zhou, Lu Li, Lijun Jin, Jian Zhou, ... Haoquan Hu
Pages 533-541

View PDF Article preview

Abstract Graphical abstract

Graphical abstract

Proposed reaction pathways of five coal-related model compounds' pyrolysis process consist of three stages: Firstly is the chain initiation, the primary decomposition process of polymer molecules produces large amounts of alkylated radicals accompanied by a small amount of residual matter through C–C bond homolysis in the thermal field. Then, the collision between free radicals and other molecules will take place during the chain propagation stage, resulting into the formation of new radicals and molecules. Lastly, annihilation of free radicals by combination with each other terminates the chain reaction. And most of the polymer samples degrade into small molecules as the released compounds, and very small amounts of heavy compounds remained as residue.

Research article Full text access

Effects of thermal dissolution in different solvents on structural characteristics and pyrolysis behaviors of lignite

Yanling Li, Sheng Huang, Youqing Wu, Shiyong Wu, Jinsheng Gao
Pages 550-557

View PDF Article preview

Abstract

Abstract

Thermal dissolution (TD) of Xilinhaote lignite (XL) in *n*-hexane, toluene and methanol were carried out, and then the residues of thermal dissolution (RTDs) and XL were pyrolyzed at a low temperature of 550 °C to explore the effect of TD on structural characteristics and pyrolysis behaviors of XL. Results show that RTDs present higher aromatic carbon content (f_a), lower aliphatic carbon (f_{al}) and oxygen-linked carbon content (f^O), indicating that the molecular structure of XL becomes more ordered after TD, especially that in *n*-hexane. Among three RTDs, the RTD in methanol obtained at 290 °C ($RTD_{M,290}$) exhibits the largest aromatic cluster size. The influences of TD at 290 °C on the pyrolysis behaviors of XL are remarkable. Compared with XL , the pyrolysis of RTDs obtained at 290 °C (RTD_{290}s) present higher char yields, lower tar, gas and water yields. The pyrolysis of RTD in *n*-hexane obtained at 290 °C ($RTD_{H,290}$) exhibits extremely low tar yield, suggesting that the low molecular weight compounds (LMWCs) isolated from XL during TD can transport into tar and/or act as hydrogen donors to stabilize the radical fragments

Research article Full text access

Fractionation of tire pyrolysis oil into a light fuel fraction by steam distillation

Guilherme Anchieta Costa, Ronaldo Gonçalves dos Santos
Pages 558-563

View PDF Article preview

Abstract

Abstract

Pyrolysis has been identified as a possible process for producing alternative fuels from thermal degradation of residue materials. In this work, a steam distillation process was applied to extract a light fuel fraction from tire pyrolysis oil. The light fuel fraction (LFF) was a light yellow, translucent liquid with a specific gravity of 0.76 g·cm^{-3} and dynamic viscosity of 0.4 mPa.s at 20 °C. LFF was mainly composed of volatile organic components of the tire pyrolysis oil. GC-MS analysis shows the light fraction composed mostly of benzene-substituted compounds (62.06%), mainly ethylbenzenes (14.84%) and methylbenzenes (13.02%) derivatives. Saturates were mainly branched alkanes containing eight carbon atoms (21.94%) and cycloalkanes in minor amount (1.35%). Olefins were essentially alkyl-branched cyclohexenes (14.66%), highlighting limonene (8.2%). The standard mid-infrared spectroscopy revealed the light fuel fraction resembles very closely the petroleum-derived gasoline. In addition, typical distillation properties (such as T50, T90, and driveability index) and octane number (Motor Octane Number and Research

Research article Full text access

NO oxidation in dry and humid conditions using hyper-cross-linked polymers: Impact of surface chemistry on catalytic conversion efficiency

Mohsen Ghafari, Ramin Ghamkhar, John D. Atkinson
Pages 564-570

View PDF Article preview

Abstract

Abstract

Microporous and hydrophobic polymers were synthesized and tested as NO oxidation catalysts to overcome water co-adsorption in combustion flue gas streams. The self-cross-linked 4,4′-bis(chloromethyl)-1,1′-biphenyl polymer (PBCMBP), with micropore volume of 0.38 cm^3/g and surface area of 1430 m^2/g, provided 62% NO oxidation efficiency at 25 °C in dry conditions but its performance dropped to 50% in the presence of 1.6 vol% moisture (wet conditions). To decrease performance loss, PBCMBP was modified with benzene (PBCMBP-BZ) to remove pendant chloromethyl groups, improving resistance to surface reactions with NO_2 that add hydrophilicity. In wet conditions, PBCMBP-BZ has 59% NO oxidation efficiency, an 18% increase compared to PBCMBP at 25 °C. PBCMBP was also functionalized with dimethylamine (PBCMBP-DMA) to increase surface basicity, increasing NO oxidation by 11% in dry conditions, but decreasing NO oxidation in wet conditions by 30% due to increased proclivity to react with NO. The combined impact of temperature and humidity was measured up to 100 °C, showing that moisture's impact

Research article Full text access

Effect of moisture content on structural evolution characteristics of bituminous coal subjected to high-voltage electrical pulses

Fazhi Yan, Jiang Xu, Baiquan Lin, Shoujian Peng, ... Xiangliang Zhang
Pages 571-578

View PDF Article preview

Abstract

Abstract

In recent years, high-voltage electric pulse (HVEP) technology has been suggested to improve the permeability of coal seams. However, the effect of moisture content on the structure evolution of coal subjected to HVEP is not clear, which restricts the wide spread application of this technology. In this study, the breakdown voltage of coal samples with different moisture content was tested, and an exponential function relationship was established between the average breakdown field strength and the moisture content of bituminous coal samples. We investigated the changes in pore structure by combing scanning electron microscopy (SEM) and nuclear magnetic resonance (NMR) results, to better understand the pore structure evolution characteristics of coal with different moisture content. Furthermore, changes in the chemical structure of the bituminous coal samples with different moisture content subjected to HVEP were investigated by Fourier transform infrared spectroscopy (FTIR). The results show that many mesopores and macropores are formed in the coal body under the action of HVEP, and the connectivity between the

Research article Full text access

Large Eddy Simulation of a particle-laden flow around a cylinder: Importance of thermal boundary layer effects for slagging and fouling

Ulrich Kleinhans, Christoph Wieland, Selahattin Babat, Hartmut Spliethoff

Pages 585-606

View PDF Article preview

Abstract Graphical abstract

Graphical abstract

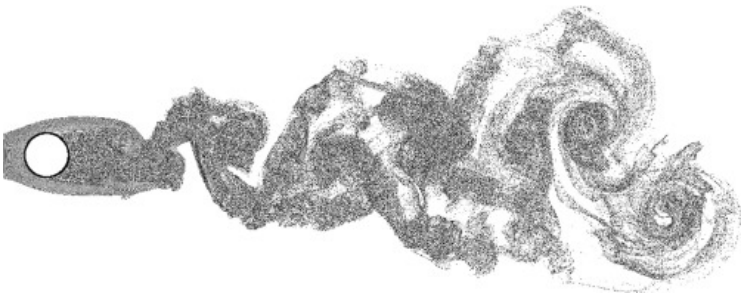

Research article Full text access

An improved Cu/ZnO catalyst promoted by Sc_2O_3 for hydrogen production from methanol reforming

Yun-Chuan Pu, Shui-Rong Li, Shuai Yan, Xiao Huang, ... Yun-Quan Liu

Pages 607-615

View PDF Article preview

Abstract Graphical abstract

Graphical abstract

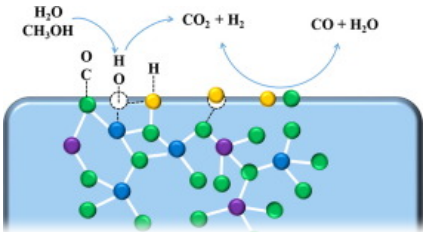

Research article Full text access

Deep oxidative desulfurization of diesel fuels using homogeneous and SBA-15-supported peroxophosphotungstate catalysts

Diana Julião, Fátima Mirante, Susana O. Ribeiro, Ana C. Gomes, ... Salete S. Balula
Pages 616-624

View PDF Article preview

Abstract

Abstract

A combination of catalytic oxidation and extraction was used for the desulfurization of a model diesel containing benzothiophene, dibenzothiophene and 4,6-dimethyldibenzothiophene, or a real diesel sample with a sulfur content of 2300 ppm. The catalysts used were the soluble peroxo compound $(n\mathrm{Bu}_4\mathrm{N})_3\{\mathrm{PO}_4[\mathrm{WO}(\mathrm{O}_2)_2]_4\}$ (PW_4) and a supported material denoted as PW_4@TMA-SBA-15 that was prepared by immobilization of PW_4 in an ordered mesoporous silica (SBA-15) derivatized with propyltrimethylammonium groups (TMA). The supported catalyst was characterized by FT-IR, FT-Raman, ^{31}P and ^{13}C MAS NMR spectroscopies, powder X-ray diffraction and scanning electron microscopy. Under optimized conditions (H_2O_2/S molar ratio = 7, 70 °C, acetonitrile as extraction solvent), both catalysts led to complete desulfurization of the model diesel within a reaction time of 2 h. The desulfurization systems could be recycled 10 times with only a slight decrease in performance being observed between the 0th and 10th oxidative desulfurization cycles. Application of the PW_4 system to the real

Research article Full text access

An ANN based hybrid chemistry framework for complex fuels

Rishikesh Ranade, Sultan Alqahtani, Aamir Farooq, Tarek Echekki
Pages 625-636

View PDF Article preview

Abstract

Abstract

The oxidation chemistry of complex hydrocarbons involves large mechanisms with hundreds or thousands of chemical species and reactions. For practical applications and computational ease, it is desirable to reduce their chemistry. To this end, high-temperature fuel oxidation for large carbon number fuels may be described as comprising two steps, fuel pyrolysis and small species oxidation. Such an approach has recently been adopted as 'hybrid chemistry' or HyChem to handle high-temperature chemistry of jet fuels by utilizing time-series measurements of pyrolysis products. In the approach proposed here, a shallow Artificial Neural Network (ANN) is used to fit temporal profiles of fuel fragments to directly extract chemical reaction rate information. This information is then correlated with the species concentrations to build an ANN-based model for the fragments' chemistry during the pyrolysis stage. Finally, this model is combined with a C_0-C_4 chemical mechanism to model high-temperature fuel oxidation. This new hybrid chemistry approach is demonstrated using homogeneous chemistry calculations of

Research article Full text access

Low temperature ignition delay times measurements of 1,3,5-trimethylbenzene by rapid compression machine

Yang Liu, Chenglong Tang, Yingtao Wu, Meng Yang, Zuohua Huang
Pages 637-645

View PDF Article preview

Abstract

Abstract

Due to the increased interest on understanding the combustion chemistry of the larger alkyl aromatic as jet fuel surrogate component, we provide new ignition delay time data of 1,3,5-trimethylbenzene/O2/Ar mixtures, for the temperature range between 880 and 1090 K, at the pressure of 20.0 and 30.0 bar and for different mixture equivalence ratio and fuel concentration, by using a well validated rapid compression machine with heating system. Measurements show that no negative temperature coefficient behavior was observed for this fuel. Subsequently, these low temperature ignition delay time data were used to validate several kinetic mechanisms including those of Gudiyella and Brezinsky (Combust Flame 2012), Diévart et al. (Fuel 2013), and Wang et al. (Combust Flame 2018), all of which significantly overestimate the reactivity of 1,3,5-trimethylbenzene in this temperature range. Sensitivity analysis at typical condition and comparisons of the rate constants of the ignition dominant reactions in different models indicate that a more complete reaction scheme for 1,3,5-trimethylbenzene (T135MB) and more

Research article Full text access

Preparation of coal-based graphene quantum dots/α-Fe_2O_3 nanocomposites and their lithium-ion storage properties

Yating Zhang, Kaibo Zhang, Kaili Jia, Guoyang Liu, ... Jieshan Qiu
Pages 646-652

View PDF Article preview

Abstract

Abstract

Nano-Fe_2O_3 particles on a nickel substrate have been obtained by electrodeposition technique adjusting the ratio of electrolyte solvent (DMF and water), and then it was used as the working electrode to obtain the C-GQDs/α-Fe_2O_3 composite material via second-step electrodeposition with the coal-based graphene quantum dots (C-GQDs) solution which had been prepared from Taixi anthracite powder as the electrolyte. The lithium-ion storage performance of C-GQDs/α-Fe_2O_3 composites as the anode in the lithium-ion battery was studied, and the results show that the composites exhibited excellent cyclability and rate capability. When the current density was 1 A/g, the specific capacitance of C-GQDs/α-Fe_2O_3 composites was up to 1582.5 mAh/g, and it could maintain 1320 mAh/g after 110 cycles. The specific capacitance was 1091 mAh/g at a high current density (5 A/g).

Research article Full text access

ASP flooding in tight carbonate rocks

Pinaki Ghosh, Himanshu Sharma, Kishore K. Mohanty
Pages 653-668

View PDF Article preview

Abstract

Abstract

Alkaline-Surfactant-Polymer (ASP) floods can mobilize oil left behind by waterfloods by lowering the interfacial tension. However, conducting such floods in tight carbonate rocks presents several challenges, e.g., polymer transport in low permeability carbonates, presence of divalent ions, geochemical interactions with chemicals and rock surface, pore-scale heterogeneity, and oil-/mixed-wettability. This paper addresses the first three challenges. A systematic study of polymer transport in low permeability carbonate cores was performed. Shearing of high molecular weight polymers and successive filtration treatment were performed to improve polymer size distribution. Single phase polymer transport experiments were performed in low permeability carbonate rocks, and optimum pretreatment method was developed. Surfactant phase behavior and aqueous stability experiments were performed to develop ultralow tension ASP and SP formulations with a reservoir crude oil. ASP and SP corefloods were performed in oil-wet low permeability limestone rocks. The oil recovery, pressure drop, effluent ionic

Research article Full text access

The role of SiO_xC_y in the catalytic performance of Co/SiC catalysts for Fischer-Tropsch synthesis

Min Wang, Shupeng Guo, Zhiwen Li, Zhongyi Ma, ... Debao Li

Pages 669-675

View PDF Article preview

Abstract Graphical abstract

Graphical abstract

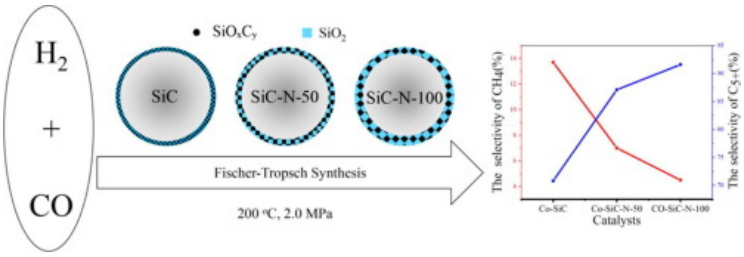

Research article Full text access

Development and validation of a reduced chemical kinetic mechanism for supercritical gasoline of GDI engine

Yukun Song, Zhaolei Zheng, Jie Xiao

Pages 676-685

View PDF Article preview

Abstract

Abstract

Supercritical combustion is a clean and efficient combustion technology that can effectively reduce particulate emissions of gasoline direct injection (GDI) engines. This study proposes a modifying mechanism for simulating supercritical gasoline; this mechanism contains 103 species and 201 reactions and is obtained by modifying the pre-exponential factors of key reactions and adding key reactions on the basis of the original mechanism proposed by our research program. The modifying mechanism is validated by a comparison with the experimental data of Fuel C, Surrogate A, Surrogate B, and each single component (iso-octane, n-heptane, and toluene). The simulation results agree with the experimental results, and the modifying mechanism can predict the various tendencies of ignition delay times with pressure and temperature. The modifying mechanism is further validated by a comparison with the detailed mechanisms proposed by Cancino and JCG et al. The comparison confirms the higher prediction accuracy of the modifying mechanism, which can promote the study of supercritical combustion process in

Research article Full text access

Bio-oil hydrotreating using nickel phosphides supported on carbon-covered alumina

Fabio Leal Mendes, Victor Teixeira da Silva, Marcelo Edral Pacheco, Fabio Souza Toniolo, Cristiane Assumpção Henriques
Pages 686-694

View PDF Article preview

Abstract

Abstract

Fast pyrolysis oil is an attractive second-generation bio-fuel. However, due to its high oxygen content, upgrading technologies are necessary to improve the properties of bio-oil. The objective of this work is to evaluate the performance of nickel phosphides supported on carbon-covered alumina (CCA) in hydrotreating of a commercial bio-oil. The effect of two different phosphides phases was investigated. The results showed that the stoichiometry of the nickel phosphide can be controlled by the weight ratio of sucrose/Al_2O_3 used in the synthesis. Two distinct catalysts can be produced: $Ni_{12}P_5$/CCA-0.7 (weight ratio of 0.7) and the Ni_2P/CC-1.4 (weight ratio of 1.4). The performances of these catalysts were compared with a commercial Ru/C. Catalytic evaluation was carried out at 250 °C and 75 bar in a batch reactor and the effect of two-step HDO (150–250 °C) was also investigated. The use of two-step HDO produced bio-oils with higher H/C ratios, indicating a higher occurrence of hydrogenation mechanisms. In addition, more thermally stable bio-oils were generated due to the significant reduction of compounds such as

Research article Full text access

Development of SO_4^{2-}–ZrO_2 acid catalysts admixed with a CuO-ZnO-ZrO_2 catalyst for CO_2 hydrogenation to dimethyl ether

Chunyanuch Temvuttirojn, Natcha Chuasomboon, Thanapa Numpilai, Kajornsak Faungnawakij, ... Thongthai Witoon
Pages 695-703

View PDF Article preview

Abstract Graphical abstract

Graphical abstract

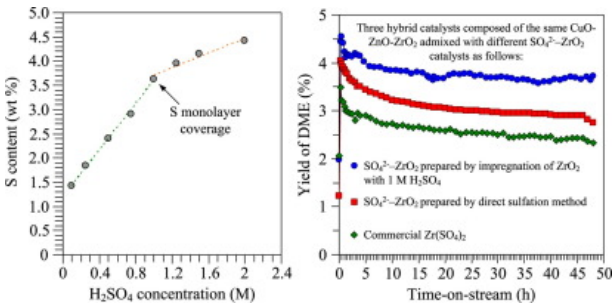

Research article Full text access

Capturing methanol and dimethoxymethane gases with ionic liquids

Hongkang Zhao, Hui Gao, Gangqiang Yu, Qunsheng Li, Zhigang Lei
Pages 704-714

View PDF Article preview

Abstract Graphical abstract

Graphical abstract

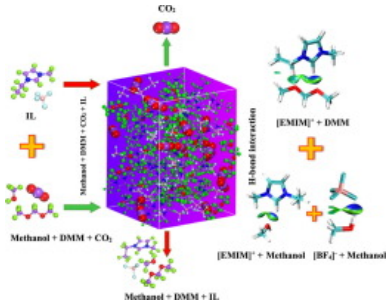

Research article Full text access

Nuclear magnetic resonance T_2 cutoffs of coals: A novel method by multifractal analysis theory

Sijian Zheng, Yanbin Yao, Dameng Liu, Yidong Cai, ... Xiawei Li
Pages 715-724

View PDF Article preview

Abstract

Abstract

Nuclear magnetic resonance (NMR) has been widely used in petrophysical characterization of coals. For NMR experimental data analysis, transverse relaxation time (T_2) cutoff value is a key parameter to identify the form of movable and irreducible fluids, and to evaluate permeability and full-scale pore size distribution (PSD). Conventionally, the T_2 cutoff value is procured by a series of centrifugal experiments, which is much complicated and time consuming, and is also hard to be used in fields such as well logging. Thus, a convenient and practical method is needed for T_2 cutoff value prediction. Based on series of centrifugal experiments, this study firstly determined an optimal centrifugal pressure of 1.38 MPa for T_2 cutoff value calculation. The results from centrifugal experiments show that the T_2 cutoff values of bituminous coals and anthracite coals in the range of 0.62–15.11 ms. Then, the multifractal analysis theory is introduced into the estimation of T_2 cutoff values of coals. The results showed that the NMR T_2 distribution of 100% water-saturated coal is multifractal, and the multifractal parameters of multifractal

Research article *Open access*

Hansen solubility parameters and thermodynamic modeling for LLE description during glycerol-settling in ester production from coconut oil

Otto Alberto Quispe Jimenez, Vanessa Vilela Lemos, Eduardo Augusto Caldas Batista, Marlus Pinheiro Rolemberg, Rodrigo Corrêa Basso
Pages 725-732

View PDF Article preview

Abstract Graphical abstract

Graphical abstract

Esters: (■) $C_{10}H_{20}O_2$; (▲) $C_{12}H_{24}O_2$; (●) $C_{14}H_{28}O_2$; □) $C_{16}H_{32}O_2$; (Δ) $C_{18}H_{36}O_2$; (♦) $C_{20}H_{40}O_2$; (◇) $C_{20}H_{38}O_2$; (○)$C_{20}H_{36}O_2$. (◀) glycerol. (▶) ethanol. (×) glycerol-rich phase. (+) ester-rich phase.

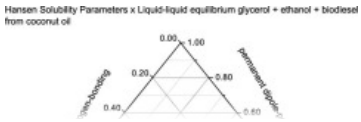

Research article Full text access

Modeling the molecular composition of vacuum residue from oil sand bitumen

Anton Alvarez-Majmutov, Rafal Gieleciak, Jinwen Chen
Pages 744-752

View PDF Article preview

Abstract Graphical abstract

Graphical abstract

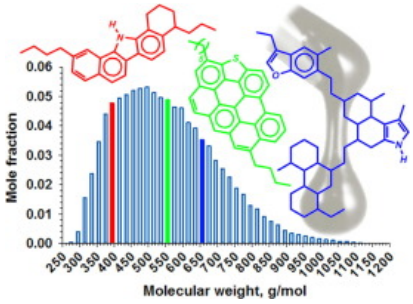

Research article Full text access

A numerical investigation of the combustion kinetics of reactivity controlled compression ignition (RCCI) combustion in an optical engine

Xinlei Liu, Sage Kokjohn, Yu Li, Hu Wang, ... Mingfa Yao
Pages 753-766

View PDF Article preview

Abstract

Abstract

This work numerically investigates the detailed combustion kinetics occurring in an optical, reactivity controlled compression ignition (RCCI) engine. Experimental data from the engine combustion network (ECN) relating to spray H and optical RCCI engine spray/combustion were used for model validation. It was found that the RCCI combustion ignition occurred in the squish, bowl rim edge, and downstream of the spray periphery. To provide insight into key reaction pathways, an in-cylinder reaction pathway analysis method was used, and four characteristic RCCI combustion features were selected: (1) initial low temperature heat release (LTHR) from the high-reactivity fuel (n-heptane) on the spray periphery; (2) intense LTHR, where both iso-octane and n-heptane were converted to intermediates (e.g., CH_2O) through oxygen-related reactions; (3) early stage high temperature heat release (HTHR) with CH_2O as the core source species; (4) and intense HTHR, characterized by a substantial energy release. Further analysis of the reactive combustion surfaces demonstrated that the interior flame structure was controlled by OH-CO-O

Research article Full text access

Facile preparation of cuprous oxide decorated mesoporous carbon by one-step reductive decomposition for deep desulfurization

Xusheng Jiang, Wenli Xu, Wei Liu, Mingbo Yue, ... Menghe Yang

Pages 777-785

View PDF Article preview

Abstract Graphical abstract

Graphic abstract

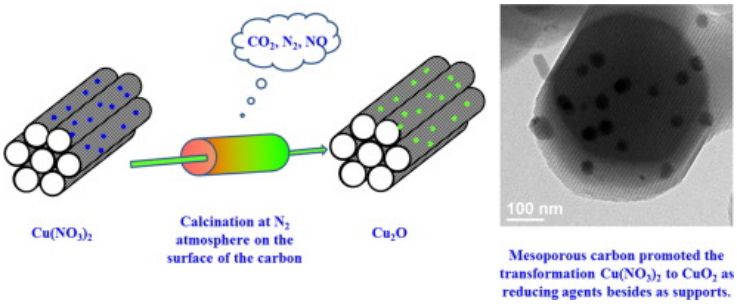

Research article Full text access

Effects of oxygen concentrations on the ignition and quasi-steady processes of n-heptane spray flames using large eddy simulation

Haiqiao Wei, Wanhui Zhao, Zhen Lu, Lei Zhou
Pages 786-801

View PDF Article preview

Abstract

Abstract

Exhaust Gas Recirculation (EGR) is a frequently used technique to reduce the production of NOx. The effect of EGR on the early flame evolution, two-stage ignition process and spray flame structures for n-heptane spray flames are investigated using large eddy simulation. The two-stage ignition process is identified based on the formation of key species and early heat release process. Results demonstrate that a longer ignition delay (ID) and flame lift-off length (LOL) under lower oxygen concentration conditions could increase the mixing time for fuel and air. However, the first-stage ignition still initiates in fuel-richer regions for the cases with higher EGR rates due to the lack of oxygen. In contrast, compared to the case with the same initial oxygen content but at a higher gas temperature of 1000 K, the first-stage ignition moves to stoichiometric mixture fraction regions at 900 K. The combustion mode analysis based on hydroxyl and formaldehyde is conducted to distinguish between the low- and high-temperature combustion regions. Most importantly, to study the stabilization mechanism, the chemical explosive mode analysis

Research article Full text access

ZIF-67 as precursor to prepare high loading and dispersion catalysts for Fischer-Tropsch synthesis: Particle size effect

Yao Chen, Xin Li, Mehar U Nisa, Jing Lv, Zhenhua Li
Pages 802-812

View PDF Article preview

Abstract Graphical abstract

Graphical abstract

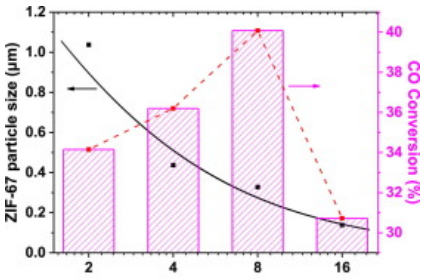

Research article Full text access

Mechanistic modelling of non-equilibrium interphase mass transfer during solvent-aided thermal recovery processes of bitumen and heavy oil

Abdullah Al-Gawfi, Hossein Nourozieh, Ehsan Ranjbar, Hassan Hassanzadeh, Jalal Abedi
Pages 813-825

View PDF Article preview

Abstract Graphical abstract

Graphical abstract

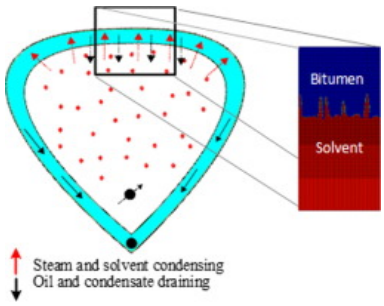

Research article Full text access

A simplified 1-butene mechanism with combined reduction method

Zemin Tian, Yingwen Yan, Jinghua Li
Pages 826-835

View PDF Article preview

Abstract

Abstract

A reduced kinetic mechanism was proposed for 1-butene based on direct relation graph related methods combined with species sensitivity analysis. At first step, sample points were identified along the temperature profiles, of which the net production rates were acquired to compute the importance index of non-target species to the targeted species. Several direct relation graph (DRG) related methods were applied to deliver simplified models of various sizes and then comparisons and interactions of these simplified models led to a compact skeletal mechanism of 82 species and 462 reactions. At next step, species sensitivity analyses were performed to carve a reduced mechanism that contains 52 species and 277 reactions out of the skeletal mechanism. Finally, the proposed chemistry model was validated against extensive kinetic experimental data. It includes ignition delay times over temperatures of 720–1800 K, pressures of 1.0–50 atm, and equivalence ratios of 0.5–2.0 measured in shock tubes and a rapid compression machine, laminar flame speeds tested at various pressures ranging 1.0 – 10 atm and at different initial temperatures

Research article Full text access

An experimental investigation and scaling analysis on flame sag of pool fire in cross flow

Xiaozheng Zhang, Xiaolei Zhang, Longhua Hu, Ran Tu, Michael A. Delichatsios

Pages 845-850

View PDF Article preview

Abstract

Abstract

Flame sag, a phenomenon observed as flame sinks downwards along the leeward sidewall, occurs for a pool fire having its rim above the ground in cross flows. Few data or investigations of this phenomenon have been reported in the literature. In the present study, the length of flame sag measured from the lowest point of sunk flame to the pool rim; as well as the critical speed of the cross flow under which the lowest point of sunk flame reaches the ground level (namely flame sag length equaling sidewall height), were quantified. Experiments were carried out by employing square quartz sand box pool fires with dimensions in the range of 10–20 cm for various cross flow air speeds, heat release rates and pool rim heights. Propane is used as the fuel. The results showed that the length of the flame sag increased with the increasing of the fire source heat release rate. And it also increased with the increasing of the air speed of the cross flow. However, the flame sag length decreased with increasing pool size. The critical air speed of the cross flow at which the flame sag reached the ground increased with increasing pool size and rim

Research article Full text access

Assembly of metallophthalocyanine-polyoxometalate hybrid for highly efficient desulfurization of organic and inorganic sulfur under aerobic conditions

Yue Li, Huaizhong Zhang, Ying Jiang, Meng Shi, ... Suiyi Zhu

Pages 861-869

View PDF Article preview

Abstract Graphical abstract

Graphical abstract

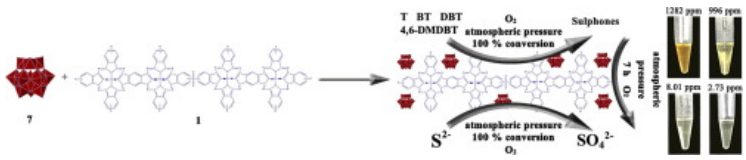

Research article Full text access

Determining the flocculation point of asphaltenes combining ultrasound and electrochemical impedance spectroscopy

Jorge Moncada, David Schartung, Natalie Stephens, Tae-Sik Oh, Carlos A. Carrero

Pages 870-875

View PDF Article preview

Abstract Graphical abstract

Graphical abstract

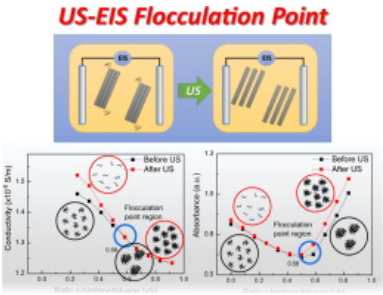

Research article Full text access

Effect of diesel-biodiesel-ethanol blends on the spray macroscopic parameters in a common-rail diesel injection system

L. Corral-Gómez, G. Rubio-Gómez, S. Martínez-Martínez, F.A. Sánchez-Cruz
Pages 876-883

View PDF Article preview

Abstract

Abstract

This work studies the viability of diesel-biodiesel-ethanol blends for compression ignition engines. Blends are prepared with a fraction of 5%, 10% and 20% of ethanol and a fraction of 10%, 20%, 30% and 40% of biodiesel in volume basis. Stability of such blends was first studied, and assessed by visually determining the phase separation 96 h after the blend was made. DB20E5, DB30E5, DB40E5, DB30E10, DB40E10 DB30E20 and DB40E20 blends maintain 0% phase separation after the test, which indicates that biodiesel acts as a surfactant and allows ternary blends being stable. For stable blends, properties (density, kinematic viscosity and surface tension) were determined. Finally, from those stable blends which properties stand within the allowed ranges by the EN-590 standard, three of them were injected in a constant volume chamber and its spray macroscopic parameters were experimentally determined. Blends with higher density show an increased spray tip penetration and those with less surface tension and kinematic viscosity show more cone angle. We conclude that DB20E10 is the blend that best air blending

Research article Full text access

Fully aerobic bioscrubber for the desulfurization of H_2S-rich biogas

Pau San-Valero, Josep M. Penya-roja, F. Javier Álvarez-Hornos, Germán Buitrón, ... Guillermo Quijano
Pages 884-891

View PDF Article preview

Abstract Graphical abstract

Graphical abstract

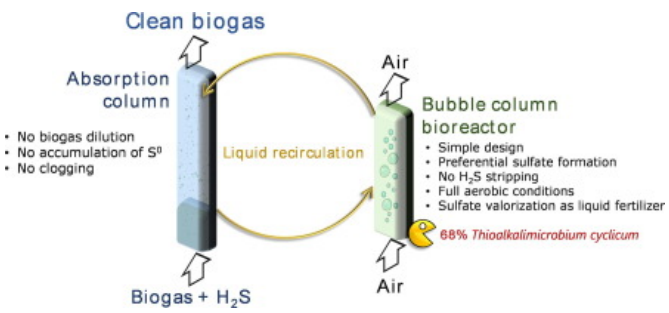

Research article *Open access*

Flash points measurements and prediction of biofuels and biofuel blends with aromatic fluids

Jinxia Fu
Pages 892-900

View PDF Article preview

Abstract

Abstract

The flash point of biofuels and petroleum fuels is an essential safety-related property for fuel processing, transportation and storage. Hydroprocessed renewable diesel (HRD-76) and synthesized isoparaffin (SIP), two biofuel blend stocks, were blended with commercial petroleum aromatic fluids (aromatic 100, 150 and 200) to investigate the impacts of aromatics on biofuel flash point and to formulate blends with identical flash point characteristics as NATO F-76 marine diesel and JP-5 jet fuel. To overcome the complexity of the fuel blends, COSMO-RS ("conductor like screening model for realistic solvation") was employed to predict the flash point of these biofuel + aromatic systems. COSMO-RS calculated the flash point of alkanes and aromatics present in biofuel and petroleum fuels and the flash point of SIP + aromatics binary mixture systems. Based on the pure compound and binary mixture predictions, COSMO-RS calculations were expanded to develop surrogate mixtures for biofuels and aromatic fluids. The surrogates were in turn utilized to predict the flash point of biofuel blends with aromatics and to

Research article Full text access

Endoscopic visualization of engine combustion chamber using diesoline, diesosene and mineral diesel for comparative spatial soot and temperature distributions

Avinash Kumar Agarwal, Yeshudas Jiotode, Nikhil Sharma
Pages 901-913

View PDF Article preview

Abstract

Abstract

Diesel engines are the prime workhorses of global transport and agriculture sectors. However, they emit significantly higher quantities of oxides of nitrogen (NOx) and particulate matter (PM). This unique study involves evaluation of in-situ spatial distribution of temperature and soot in the engine combustion chamber using high-temperature endoscopy, while the engine was being fuelled with emerging fuels so that suitable strategies for effective control of emissions could be devised. Two new test fuels namely diesosene (K20) (20% kerosene (v/v) blended with mineral diesel) and diesoline (G20) (20% gasoline (v/v) blended with mineral diesel) were compared with the baseline mineral diesel in a conventional direct injection compression ignition (DICI) engine. These two fuels represent relatively inferior quality diesel, which is increasingly available in global markets due to gradually exhausting petroleum resources and is produced from heavier/residual crude left in the oil wells. Diesoline showed superior combustion characteristics compared to diesel and diesosene. Endoscopic visualization technique emerged to be an

Research article Full text access

Pore structure variations across structural deformation of Silurian Longmaxi Shale: An example from the Chuandong Thrust-Fold Belt

Hongjian Zhu, Yiwen Ju, Cheng Huang, Kui Han, ... Jin Qian
Pages 914-932

View PDF Article preview

Abstract

Abstract

Pore types and pore size vary systematically across structural deformation in the shale gas reservoirs but lack a comprehensive study. Twelve Longmaxi Shale samples spanning a tectonism range from undeformed to deformed were formed in the structural deformation zone located in a field section of the Chuandong Thrust-Fold Belt, South China. Herein, pore structure investigations are performed using three types of organic-rich shale (undeformed shale, fault-related shale, and fold-related shale) with vitrinite reflectance (R_o value) ranging between 1.90 and 2.57% and total organic carbon (TOC) content ranging between 2.25 and 4.40%. Compared to the undeformed shales, deformed samples are quartz rich and carbonate poor. Total porosity from mercury intrusion porosimetry (MIP) ranges between 3.74 and 5.62% in undeformed shales, 2.66–6.83% in fold-related shales, and 2.55–13.92% in fault-related shales. Scanning electron microscopy (SEM) study of the pore type evolution reveals organic matter (OM) pores are dominant in undeformed shales whereas the interparticle (interP) pores, intraparticle

Research article Full text access

Ex-situ catalytic fast pyrolysis of Beetle-killed lodgepole pine in a novel ablative reactor

Heather G. Wise, Anthony B. Dichiara, Fernando L.P. Resende

Pages 933-940

View PDF Article preview

Abstract Graphical abstract

Graphical abstract

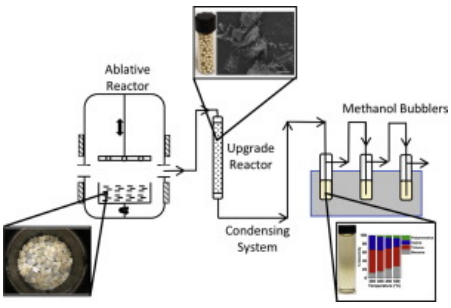

Research article Full text access

Effect of electric charge and temperature on the near-field atomization of diesel and biodiesel

G. Singh, P.X. Pham, A. Kourmatzis, A.R. Masri

Pages 941-953

View PDF Article preview

Abstract

Abstract

High speed backlight imaging combined with particle tracking velocimetry is used to analyse the near-field characteristics of a series of typical charge injection atomizer sprays. Diesel and biodiesels are studied as a function of applied voltage and temperature, in order to provide new information on the influence of fuel preheating on charged sprays. Detailed quantitative characterisation of ligament and droplet statistics, fragment orientation and local dimensionless scalings using “effective surface

tension" are presented. These shed new light on the fragmentation mechanisms that drive primary atomization in charge injection systems. It is observed that pre-heating can reduce the droplet size of electrostatically atomized dielectric fluids. However, the advantage of pre-heating is limited by a higher ionic mobility at higher temperatures which increases the leakage current. Bimodality in the droplet size distribution is noted which confirms previous work, and this study extends the literature

Research article Full text access

Biohydrogen production using a granular sludge membrane bioreactor

Germán Buitrón, Karla M. Muñoz-Páez, Christian E. Hernández-Mendoza
Pages 954-961

View PDF Article preview

Abstract

Abstract

Biohydrogen was produced using a granular biomass reactor coupled to a submerged internal membrane. The reactor performance was evaluated under different organic loading rates (OLR) ranging from 5 to 60 $g\,L^{-1}d^{-1}$ and hydraulic retention times (HRT) from 5.5 to 1.25 h. The UASB reactor was operated at 35 °C and pH 4.5. It was observed that the membrane introduction to the reactor does not affect the granule size or integrity. The maximum hydrogen production rate was obtained at 30 $g\,L^{-1}d^{-1}$ and 4 h of HRT ($475 \pm 15\,mLH_2\,L^{-1}h^{-1}$). A further increase of the OLR resulted in a lower hydrogen production due to a shift of the metabolism to solvent production. The use of membranes allowed the application of relatively low HRT; however, HRT lower than 2 h promoted the homoacetogenic metabolism, decreasing the hydrogen production. The results indicate that the membrane fouling is not only affected by the total EPS formed but also by the operational flux applied.

Research article Full text access

Influence of silica nanoparticles on heavy oil microrheology via time-domain NMR T_2 and diffusion probes

Heng Wang, Esteban A. Taborda, Vladimir Alvarado, Farid B. Cortés
Pages 962-972

View PDF Article preview

Abstract

Abstract

The objective of the present work is to determine the effect of silica nanoparticles on the microrheological properties of heavy and extra-heavy crude oils using time-domain nuclear magnetic resonance (TD-NMR) methods. Three heavy crude oils with different asphaltene contents were studied. The oils steady-state rheograms were collected as a function temperature and nanoparticles concentration. Transverse relaxation time (T_2) and diffusion coefficient measurements were used as probes of the crude oils microrheological responses. A clear inverse correlation between either the log-mean T_2 ($\mathbf{T_{2,LM}}$) or the diffusion coefficient and the rheometric oil viscosity in the presence of nanoparticles was found. Results further show the likely existence of an optimal concentration of nanoparticles in the vicinity of 1000 mg/L. The maximum viscosity reduction of roughly 35–45% was observed for the three heavy crude oils. The heavy oil refractive index decreases after the oil was placed in contact with nanoparticles, confirming adsorption of polar material on nanoparticles. T_2 and the diffusion coefficient increase in the apparent region of

Research article Full text access

Experimental studies on two dimensional particle swarm gasification of different coal chars and petroleum coke at high temperature

Ming Liu, Zhongjie Shen, Qinfeng Liang, Jianliang Xu, ... Haifeng Liu
Pages 973-984

View PDF Article preview

Abstract

Abstract

In this study, the effects of particle concentration on particle temperature and gasifying agent concentration was analyzed based on the gasification experiments. The gasification processes of different coal chars and petcoke were divided into fast reaction process (gasification of lignite and bituminous char) and slow reaction process (gasification of anthracite char and petcoke). The reactivity index of fast reactions was extremely higher than that of slow reactions. The reaction rate of sparse particle swarms also differed from that of dense particle swarms for the same sample. For fast reactions, the effects of particle concentration on gasification reactivity was limited. It was illustrated that the evident increase of particle temperature and the decrease of gasifying agent played a contrary effect on reactivity for fast-reaction samples. Nevertheless, the slight decrease of particle temperature and evident decrease of gasifying agent concentration led to the decrease of reaction rate with particle concentration for slow-reaction samples

Research article Full text access

Production and use of biofuels for transport in Poland and Brazil – The case of bioethanol

Joanna Mączyńska, Małgorzata Krzywonos, Adam Kupczyk, Karol Tucki, ... Izabela Wielewska
Pages 989-996

View PDF Article preview

Abstract

Abstract

The objective of this paper was to compare the markets and methods of production of ethanol to be used in transport in Poland and Brazil. Differences in terminology associated with its use for transport purposes in both countries have been discussed, as well as the market-related aspects of such use, comparing, among other things, the scale of production and use in years 2010–2016 and presenting the results of research on attractiveness (value) of the market of transport biofuels (especially bioethanol) in Poland, which were compared to the perspectives of market development in Brazil.

In Brazil, the share of renewable energy in total energy consumption is at the level of 42%, making it a world leader in use of energy from RES (renewable energy sources). 18% of the energy used is sugarcane bioenergy (bioethanol). At present, most of this production is being consumed by the domestic market, where ethyl alcohol is being sold as a pure ethanol fuel or mixed with

Research article Full text access

Adsorptive removal of nitrogen-containing compounds from fuel over hierarchical porous aluminosilicates synthesized by kinetic regulation method

Jiang-An You, Haiyan Song, Jin Zhang, Chunxia Chen, Fuqin Han
Pages 997-1007

View PDF Article preview

Abstract Graphical abstract

Graphical abstract

Construction of hierarchical porous Al-KIL-2 via kinetic regulation.

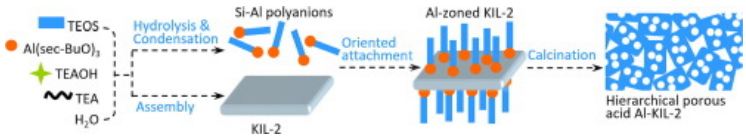

Research article *Open access*

Poisoning effects of H_2S and HCl on the naphthalene steam reforming and water-gas shift activities of Ni and Fe catalysts

Xiaomin Dou, Andrei Veksha, Wei Ping Chan, Wen-Da Oh, ... Teik-Thye Lim
Pages 1008-1018

View PDF Article preview

Abstract

Abstract

H_2S and HCl are common impurities in raw syngas produced during gasification of biomass and municipal solid waste. The purpose of this study was to investigate the poisoning effect of H_2S and HCl on synthesized and commercial catalysts during steam reforming of naphthalene. Four synthesized catalysts with different loadings of Ni and Fe on alumina support and two commercial catalysts were selected and evaluated in a fixed bed reactor at 790, 850 and 900 °C. The obtained results revealed that reforming and water-gas shift (WGS) activities of catalysts did not benefit from the Fe addition. The activities were influenced differently by H_2S and HCl indicating that the reactions were catalyzed by different active sites on the nickel surface. In the presence of H_2S and HCl, the poisoning of naphthalene reforming activity was caused by H_2S and was not affected by HCl when both compounds were present in the gas. H_2S chemisorbs on nickel surface forming NiS and decreasing the accessibility of active sites to hydrocarbons. The poisoning effect was only partially reversible. On the contrary, the poisoning of WGS activity

Research article Full text access

Dissociation behaviors of coal-related model compounds in ionic liquids

Zhiping Lei, Lin Dong, Shigang Kang, Yaqin Huang, ... Chunxiu Pan
Pages 1019-1025

View PDF Article preview

Abstract

Abstract

Ionic liquids have demonstrated to be promising solvents for processing coal and biomass. Aiming to exploit ionic liquids (ILs) as media for degradation of coal, diphenylmethane (DPM), diphenyl ether (DPE), and diphenyl ketone (DPK) were used as coal-related compounds to study the degradation behaviors of weak-bond structures of coal in ionic liquids in this work. It was found that 1-sulfonic acid butyl-3-methylimidazolium 14 trifluoromethanesulfonate ([B(SO3H)mim]OTf), 1-ethyl-3-methylimidazolium acetate ([Emim]Ac) and 1-butyl-3-methyl-imidazolium chloride ([Bmim]Cl) have a significant effect on the thermal dissociation

of the model compounds. [B(SO_3H)mim]OTf has a significant effect on the cleavage of DPM and DPK. [Bmim]Cl promotes the cleavage of the DPE. The dissociation effect of the model compound under the action of ionic liquid increases with the increase of reaction temperature. The interaction between the oxygen-containing functional groups in the model compound promotes the

Research article Full text access

Solubility of hydrocarbon and non-hydrocarbon gases in aqueous electrolyte solutions: A reliable computational strategy

Niaz Neisani Samani, Sayed Mohammadreza Miforughy, Hossein Safari, Omid Mohammadzadeh, ... Sohrab Zendehboudi
Pages 1026-1035

View PDF Article preview

Abstract

Abstract

Determining solubility of hydrocarbon and non-hydrocarbon components of natural gas is crucial for theoretical studies and engineering design. In this study, new solubility prediction models were developed for both hydrocarbon gases (methane, ethane, propane, and butane) and non-hydrocarbon gases (CO_2 and N_2) in aqueous solutions of strong electrolytes using a hybrid modeling strategy, which links the Coupled Simulated Annealing (CSA) to the Least-Squares Support Vector Machine (LSSVM) technique. Comparing the models' predictions with experimentally determined solubility values, a very good agreement was noticed, leading to the overall correlation coefficients of 0.9880 and 0.9907 for the hydrocarbon and non-hydrocarbon gases, respectively. These models were also found to succeed in capturing the physical trends among experimental datasets through performing sensitivity analysis between the dependent and independent parameters. Developed models can be utilized to predict the solubility of pure and/or a mixture of hydrocarbon and non-hydrocarbon gases in aqueous electrolyte solutions, covering

Research article Full text access

Porosity and storage capacity of Middle Devonian shale: A function of thermal maturity, total organic carbon, and clay content

Liaosha Song, Keithan Martin, Timothy R. Carr, Payam Kavousi Ghahfarokhi
Pages 1036-1044

View PDF Article preview

Abstract

Abstract

Porosity and pore size distribution (PSD) are critical reservoir parameters. Pore surface area, pore volume, PSD, and porosity were measured using subcritical nitrogen (N_2) adsorption, and helium porosimetry. A suite of 17 samples were collected from 4 wells in Pennsylvania and West Virginia to analyze the evolution of porosity with increasing thermal maturity in Middle Devonian shales of the Appalachian Basin. The thermal maturity of the tested samples covers a wide range in the hydrocarbon generation sequence from wet gas/condensate zone (vitrinite reflectance (R_o) = 1.16%) to post-mature zone (R_o = 2.79%). Shale samples from the Marcellus Shale and Mahantango Formation used in this study have total organic carbon contents from 0.41 to 7.88 wt%. Results indicate that total organic carbon (TOC) has the strongest effect on porosity and pore structure. The presence of organic matter in shale strongly enhances the storage capacity by increasing the specific surface area and pore volume, which represents sorption storage capacity and free-gas storage capacity. Differences in porosity and pore structure have a complex

Research article Full text access

Influence of blending and hot water extraction on the quality of wood pellets

Mark H. Eisenbies, Timothy A. Volk, Tom E. Amidon, Shun Shi
Pages 1058-1067

View PDF Article preview

Abstract

Abstract

In order to meet the projected demand for biomass feedstocks, multiple sources will be needed. Biomass feedstocks are often have a high degree of variability with regards to important properties such as ash, moisture, and energy content. The efficiency of conversion processes may be sensitive to this variability; thus, strategies are needed to ensure that consistent and reliable feedstocks are produced that meet end-user specifications. The objective of this study was to examine the effect of source, blending and hot water extraction (HWE) on the quality of wood pellets. Debarked maple biomass was blended at various rates with whole stem harvested willow, HWE willow, and HWE maple biomass, made into pellets and then compared to existing ISO (17225) pellet standards. Untreated willow pellets were unable to consistently meet key specifications such as ash and moisture. However, pellets blended with either HWE willow, maple or HWE maple at rates between 20 and 50 percent willow still met the most stringent requirements. HWE decreased the ash content of willow below 1% and was on par with untreated maple. HWE

Research article Full text access

Effect of air jet momentum on the topological features of turbulent CNG inverse jet flame

S. Mahesh, D.P. Mishra
Pages 1068-1075

View PDF Article preview

Abstract

Abstract

Inverse jet flame (IJF) configuration is a variant of coaxial nonpremixed jet flame which can produce a nonluminous compact blue flame with independent control of air and fuel jet momentum. In the present work, the effect of central air jet velocity on visible topological features such as, visible flame height and base flame height is investigated experimentally. Also the fluid dynamics behind the evolution of base flame in IJF configuration is unraveled in this study. Notably, buoyancy induced oscillations of IJF, which is relatively unexplored in open literature is studied in this work. Moreover, a systematic classification of IJF based on the evolution of its visible flame features with variation in the central air jet and annular fuel jet velocities is reported. In addition, a semi-empirical correlation for visible flame height of IJF with air-fuel momentum ratio is arrived in the present work which can be useful in the design of IJF based burners utilized for impingement heat transfer applications.

Research article Full text access

Evaluation of solvents for in-situ asphaltene deposition remediation

Jun Kuang, Josiah Yarbrough, Shayan Enayat, Nigel Edward, ... Francisco M. Vargas
Pages 1076-1084

View PDF Article preview

Abstract

Abstract

Upon the formation and the accumulation of the deposits, cost-effective cleaning strategies should be applied to remediate and remove the organic solids. The injection of aromatic solvents, usually know as solvent wash, is one of the commonly used techniques to re-dissolve the deposited asphaltenes in the well. To select and develop the best solvents and the most appropriate solvent soaking conditions for asphaltene remediation, a re-dissolution test apparatus using a packed bed column was introduced to evaluate the solvents for in-situ asphaltene deposition remediation under more realistic production conditions. The solvency power of three aromatic solvents and four commercial solvents was determined and compared. Under the current experimental conditions, the injection of *p*-xylene re-dissolves 31.3% and 69.8% more deposits than the same volume of toluene and aromatic naphtha (A150). Additionally, the solvent wash by toluene/diesel mixture (50/50 by volume) and diesel significantly reduces the re-dissolution efficiency by 31.1% and 74.3% by comparing to toluene. Results also suggest that the screening of chemical solvents

Research article Full text access

Comparison of single particle combustion behaviours of raw and torrefied biomass with Turkish lignites

Duarte Magalhães, Aidin Panahi, Feyza Kazanç, Yiannis A. Levendis
Pages 1085-1094

View PDF Article preview

Abstract

Abstract

This study investigated the combustion behaviour of single pulverized biomass and lignite coal particles under high temperature–high heating rate conditions. Selected fuels included three important agricultural residues in Turkey (olive residue, almond shell, and hazelnut shell), and two lignite coals from the regions of Tunçbilek and Soma in Turkey. Biomass fuels were either raw or torrefied at 275 °C for 30 min in nitrogen. The biomass fuels were sieved to a size cut of 212–300 μm, and the coals were sieved to 106–125 μm. An optically-accessible drop tube furnace, operated at a wall temperature of 1400 K, was used to burn single fuel particles in air. High-speed cinematography and three-colour pyrometry were used to characterise the combustion behaviour of the fuel particles. All biomass particles ignited homogeneously forming large and circular volatile matter envelope flames, followed by distinct char combustion phases. The Tunçbilek lignite also ignited homogeneously and burned in two combustion stages, first forming bright sooty and elongated flames with contrails, upon extinction of which char combustion

Research article Full text access

Investigating auto-ignition behavior of *n*-heptane/*iso*-octane/ethanol mixtures for gasoline surrogates through rapid compression machine measurement and chemical kinetics analysis

Qinhao Fan, Zhi Wang, Yunliang Qi, Yingdi Wang
Pages 1095-1108

View PDF Article preview

Abstract

Abstract

Overall ignition delay time (OID) is used as indicator to characterize reactivity and anti-knock quality of fuel. In this work, both experimental measurement and modeling work have been conducted to evaluate OID properties for six ternary blends comprising *n*-heptane/*iso*-octane/ethanol. Experimental measurement was performed in a rapid compression machine, while modeling work was based on the gasoline surrogate mechanism. The decoupling study on research octane number (RON)/motor octane number (MON) and octane sensitivity (S) has been carried out by adjusting fuel composition. The thermal conditions of experiments cover low-to-medium temperatures from 640 K to 740 K and pressures from 9.5 bar to 21 bar. Oxygen is utilized as the oxidizer while nitrogen and argon are regarded as the buffer gas to adjust thermal conditions. Combined with chemical

kinetics analysis, negative temperature coefficient (NTC) behavior in the experiment is entirely attributed to *iso*-octane and the

Research article Full text access

Nitrogen conversion during the homogeneous and heterogeneous stages of sludge steam gasification: Synergistic effects of Fenton's reagent and CaO conditioner

Geng Lu, Huan Liu, Qiang Zhang, Jiaxing Wang, ... Hong Yao
Pages 1109-1116

View PDF Article preview

Abstract Graphical abstract

Graphical abstract

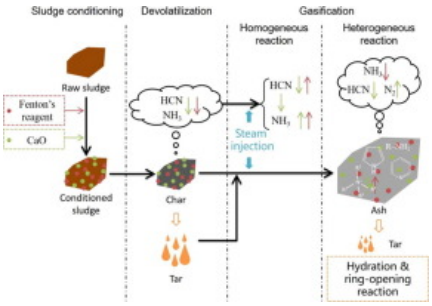

Research article Full text access

Surfactant flooding in oil-wet micromodels with high permeability fractures

Lucas Mejia, Mohsen Tagavifar, Ke Xu, Miguel Mejia, ... Matthew Balhoff
Pages 1117-1128

View PDF Article preview

Abstract

Abstract

Recovery in carbonate reservoirs is challenging because they are often oil wet and highly fractured. Surfactant flooding has been proposed as a possible enhanced oil recovery method to address these problems. To better understand the mechanisms of oil recovery from oil-wet, fractured rocks using surfactants, we created oil-wet glass micromodels, traversed by a deep fracture (130 μm) and conducted surfactant spontaneous imbibition experiments and floods at typical reservoir flow rates (approximately 2 ft/day). We compared the effects of capillary, viscous, and gravity forces as well as wettability alteration. We show, by conducting spontaneous imbibition experiments with negligible gravity effects (inverse Bond number ~10^5) and by analyzing the results using simple force balance calculations, that in our micromodels low IFT plays the key role in balancing the viscous, gravity, and surface forces and hence the dynamics of imbibition. To quantify the role of viscous forces, we present displacement experiments at low IFT (10^{-3} mN/m) where transverse viscous pressure gradients mobilize oil from the matrix into the fracture

Research article Full text access

Comparative studies on the structural features of soluble portions from thermal dissolution/methanolysis and catalytic hydroconversion of an extraction residue from Heishan lignite

Zheng Yang, Xian-Yong Wei, Zhi-Xin Li, Min Zhang, ... Zhi-Min Zong
Pages 1138-1144

View PDF Article preview

Abstract

Abstract

Heishan lignite (HL) was extracted with isometric acetone/carbon disulfide mixed solvent under ultrasonic irradiation. The extraction residue (ER) was subjected to thermal dissolution/methanolysis (TD/M) in methanol and catalytic hydroconversion (CHC) in cyclohexane (CH) at 300 °C under 1 MPa of N_2 over a supported acid (SA). The methanol-soluble portion (MSP) from the TD/M and CH-soluble portion (CHSP) from the CHC were analyzed with a gas chromatograph/mass spectrometer (GC/MS) and Fourier transform infrared (FTIR) spectrometer, while ER and the residues from the TD/M ($R_{TD/M}$) and CHC (R_{CHC}) were characterized with the FTIR spectrometer and an X-ray photoelectron spectrometer (XRPES). The results show that the yields of MSP and CHSP are *ca.* 22.6% and 16.1%, respectively. According to the analysis with GC/MS, CHSP is rich in tetramethylbenzenes and dimethylnaphthalenes, while most of the GC/MS-detectable compounds in MSP are xylenols, trimethylphenols, and methyl normal alkanoates. During the TD/M, the cleavage of some C—O bonds could be the main

Page 1 of 2

Previous vol/issue Next vol/issue

ISSN: 0016-2361